AD_____

Award Number: **W81XWH-07-1-0716**

TITLE: **Neuroprosthetics and Solutions for Spinal Cord Dysfunctions**

PRINCIPAL INVESTIGATOR: Douglas Weber, Ph.D.

CONTRACTING ORGANIZATION: University of Pittsburgh

Pittsburgh, PA 15260

REPORT DATE: August 2012

TYPE OF REPORT: Final

PREPARED FOR: U.S. Army Medical Research and Materiel Command
Fort Detrick, Maryland 21702-5012

REPORT DOCUMENTATION PAGE

Form Approved
OMB No. 0704-0188

1. REPORT DATE *(DD-MM-YYYY)*	2. REPORT TYPE	3. DATES COVERED *(From - To)*
August 2012	Final	1 January 2008 - 31 July 2012

4. TITLE AND SUBTITLE
Neuroprosthetics and Solutions for Spinal Cord Dysfunctions

5a. CONTRACT NUMBER

5b. GRANT NUMBER
W81XWH-07-1-0716

5c. PROGRAM ELEMENT NUMBER

6. AUTHOR(S)
Douglas Weber, PhD, PI
Jon Pearlman, PhD, Co-I
Wei Wang, PhD, Co-I
Rory Cooper, PhD, Co-I
Tracy Cui, PhD, Co-I

5d. PROJECT NUMBER

5e. TASK NUMBER

5f. WORK UNIT NUMBER

7. PERFORMING ORGANIZATION NAME(S) AND ADDRESS(ES)
University of Pittsburgh
Office of Research
350 Thackeray Hall
Pittsburgh, PA 15260

8. PERFORMING ORGANIZATION REPORT NUMBER

9. SPONSORING / MONITORING AGENCY NAME(S) AND ADDRESS(ES)
U.S. Army Medical Research
Fort Detrick, Maryland

10. SPONSOR/MONITOR'S ACRONYM(S)

11. SPONSOR/MONITOR'S REPORT NUMBER(S)

12. DISTRIBUTION / AVAILABILITY STATEMENT
Approved for public release; distribution unlimited

13. SUPPLEMENTARY NOTES

14. ABSTRACT
This project is focused on the development of a radically new class of prosthetic devices that will mimic more closely the full range of sensory and motor capabilities of natural limbs. To this end, we have made significant progress on four integrated projects to advance the development of neuroprosthetic limbs including: 1) creation of a sensory neural interface to provide amputees with tactile and kinesthetic feedback from their prosthetic limb, 2) improving the biocompatibility of implanted neural interface electrodes, 3) development of a virtual reality training and testing system for neuroprosthetic limbs, and 4) development of prosthetic hardware testing equipment and procedures. To date, we have completed experiments to characterize the organization of sensory neurons in the DRG for the creation of a sensory feedback neural interface and evaluated the brain's response to sensory stimulation. We have also completed experiments to evaluate histologically the tissue response to electrodes implanted chronically in DRG, dorsal roots, and spinal cord. We have designed and developed a virtual reality training system based on custom software developed in-house for training amputees to operate myoelectric and neurally controlled prosthetic limbs. Finally, we have developed a test jig to determine compliance with ISO standards for prosthetic hardware, and we have begun testing prosthetic feet.

15. SUBJECT TERMS
neural interface, neural prosthesis, biocompatibility, virtual reality, amputee, sensory feedback

16. SECURITY CLASSIFICATION OF:			17. LIMITATION OF ABSTRACT	18. NUMBER OF PAGES	19a. NAME OF RESPONSIBLE PERSON
a. REPORT	b. ABSTRACT	c. THIS PAGE			USAMRMC
U	U	U	UU	52	19b. TELEPHONE NUMBER *(include area code)*

Table of Contents

Introduction

Advances in body armor and life-saving technology have increased survival rates of severely injured military personnel. Unfortunately, the survivors of improvised explosive devices used in gulf conflicts are often left with amputations and/or spinal cord injuries. The increase in amputations and paralysis among military personnel requires significant advances in prosthetics and functional electrical stimulation (FES) systems such that the soldiers can return to the field if they desire or to productive civilian lives. This project is focused on the development of a radically new class of prosthetic devices that will mimic more closely the full range of sensory and motor capabilities of natural limbs. By providing a communication link between the prosthesis and the user's nervous system, our goal is to integrate the prosthetic limb as a natural component of the user's sensorimotor apparatus. Significant progress has been made toward this goal, but there is still much work to be done, particularly in the areas of restoring sensory feedback, improving the electrode-neuron interface, user-training, and prosthetic durability. Project 1 deals directly with the issue of providing somatosensory input to soldiers with amputation or paralysis. Project 2 deals with improving the chronic stability of the neural interface and will test novel polymer surface modification methods for improving the long-term reliability of the implanted microelectrodes. Although neural control is the ultimate goal of our work, we believe that there is useful control information available in the muscles of the residual limb. Project 3 uses virtual reality to place patients in an environment with a simulated neuroprosthesis. In this environment, we can discover the degree of remaining electromyographic (EMG) signal content and begin to train patients to control their neuroprosthetic. In this way, the virtual environment serves two important purposes: 1) testing algorithms for myoelectric and/or neural control, and 2) training the user on neuroprosthetic control. This new class of prosthetic devices will literally look, feel, and function like natural limbs, but their internal construction will include complex machinery, motors, sensors, and control instrumentation. Therefore, durability is a major concern, especially since users will be more able to engage in rigorous physical activities. Through our interactions with soldiers returning to duty after amputation, we know that current prosthetics do not stand up to the harsh use of active amputees. Project 4 is designed to rigorously test currently available and newly design prosthetics to understand the components that fail and the ways to remediate these failures. In addition, we will build devices that can track prosthetic use and thus provide information on the use in terms of both distance traveled and force imparted.

Summary of Major Accomplishments in each Project

Project 1

The first project is aimed at creating a sensory neural interface for restoring tactile and proprioceptive sensations to users of neuroprosthetic limbs. We have developed a novel approach in targeting primary afferent neurons at the level of the DRG, a focal and mechanical protected target for accessing a large population of sensory neurons near their point of entry into the CNS. We are the first group to target stimulation of sensory neurons with penetrating microelectrodes in the DRG. Results from this project have not only demonstrated the feasibility of this approach, but have also established a solid foundation of knowledge in understanding how stimulation parameters affect the number and types of neurons that are recruited by DRG microstimulation. In addition, we have made important discoveries into the effects of various stimulation parameters on the activity of CNS neurons. This knowledge is crucial for designing stimulation patterns that are effective in delivering natural and useful sensory inputs to the user. Although it is impossible to directly measure a 'sensory experience', we have developed a novel experimental approach for quantifying the information conveyed by variations in the basic parameters of stimulation. As such, we are able to discover those stimulation conditions which achieve the most meaningful delivery of sensory information to the user. As our goal is to develop a permanent sensory neural interface for patients, we have also begun experiments to test the chronic reliability of a sensory neural interface in the DRG. Further studies of this type will establish safe and reliable technology and procedures for humans.

Project 2

The implanted neural interface must remain stable throughout the lifespan of the user, but immune and inflammatory reactions at the implant site are known to degrade the performance of implanted microelectrodes. Since tissue reactions vary in different parts of the nervous system, our objectives are 1) to examine the tissue responses around electrodes implanted in the DRG and spinal cord 2) to test whether surface coating, with agents that encourage specific neuronal survival and growth and reduce inflammation, will be effective in improving the biocompatibility and 3) to examine the effect of chronic stimulation on surrounding tissue. In the first two years of the project, we have optimized the probe implantation, tissue processing and quantification protocols, developed neuron promoting L1 coating and electrically controlled dexamethasone release coatings. In the past year, we have completed the chronic implantation and histology study. Extensive characterization of the cellular tissue response around the electrodes in DRG and SC at both acute and chronic time points was performed. The effect of the L1 coating was evaluated in vivo, and encouragingly the L1 coating showed trends of reduced microglia/macrophage activation and kill zone size. A novel PEDOT/carbon nanotube coating was developed for the stimulating electrodes. This coating can be directly deposited on the electrode sites and improve the impedance and charge injection capacity of the electrodes by several orders. Such properties are expected to induce less tissue damage caused by chronic stimulation. In addition, anti-inflammatory drug can be released during the stimulation to further protect the neurons and reduce scarring.

Project 3

The central theme of the third project is to both develop advanced virtual reality (VR) environment for prosthetic arm user training and to demonstrate the effectiveness of such VR environment using clinically-relevant studies. From the engineering development perspective, this project contributed uniquely in the following areas. First, we have developed a complete VR environment for prosthetic arm training. It includes a fully animated avatar with a high degree of freedom across the whole body. The arm and hand specifically have all the degrees of freedom a real human arm has, and they are rendered with a high polygon count for vivid simulation.

This VR environment can be easily controlled via its standard network interface. Second, we have developed a complete human-machine interface software package, named “Craniux”, is developed in house. This is an open-source, open-platform, modular software package developed using National Instruments LabVIEW programming language. It allows any developers and researchers interested in real-time human-machine interface, especially brain-machine interface, applications to quickly and effectively prototype various physiological signal processing algorithms and control paradigms. This software serves as central software for all our current on-human primate and human subject research projects. Third, we have developed a unique software tool, rtMEG, for real-time access of magnetoencephalography (MEG) signals. The state-of-the-art whole-head MEG system (Elekta Neuromag) is gaining significant popularity globally in many clinical and research labs. However, previously, it is not possible to access MEG signals in real-time from a third-party computer for any customized real-time signal processing and applications. In collaboration with engineers at Elekta Neuromag, we are the first group to develop a software toolbox that provides real-time MEG signal access. Fourth, we have conducted clinically relevant studies with the abovementioned software tools and demonstrated:

Human subjects can be trained effectively with our VR environment for controlling virtual prosthetic limbs. Specifically, a new concept, “synergy-based control”, was introduced by us that allowed an individual to control dexterous hand movement with a limited number of control channels (e.g. a few surface electromyographic electrodes). We have observed robust sensorimotor activity for both overt and observed hand movement using MEG, and our software enabled us to train a neural decoder for real-time control of a virtual arm using MEG signals. Last but not the least, we were able to use the VR environment in our most recent clinical study where an individual with tetraplegia were trained to use his brain signals (electrocorticographic (ECoG) signals) to control the movement of virtual cursors and prosthetic limbs. This is the first demonstration of ECoG control in an individual with tetraplegia. Furthermore, we were able to directly transfer the control from the virtual environment to a real prosthetic arm, demonstrating the feasibility and advantage of user training using a VR environment for eventual operation of physical prosthetic limbs.

Project 4

One of the major accomplishments of the prosthetic testing portion of the study was the expansion of the available prosthetic knowledge and literature. The conclusion, reported in the peer-reviewed journal Prosthetics and Orthotics International, that the heavy duty prosthetic feet prescribed to active users, such as athletes and military personnel, investigated in this project meet the ISO 10328 standards. This indicates that the manufacturers of these feet may hold themselves to these voluntary standards, which help ensure that prosthetic foot users have access to durable, high quality products. Over the course of the prosthetic foot testing portion of the project, the investigators were able to design and develop testing devices, fixtures, protocols, and techniques for prostheses, which were reported at a conference of the Rehabilitation Engineering Society of North America and a Walter Reed Army Medical Center State of the Science Symposium, which can be applied to future studies in order to shed even more light on the durability and robustness of prosthetic foot components. These future studies may include expanding upon the ISO standards to include exposing the prostheses to torsional loading, moisture, and extreme temperatures. The knowledge and skills gained from this project will also allow investigation into the efficacy of other assistive technology, such as wheelchair components, Paralympic sporting equipment, and other devices used by individuals with disabilities.

Body

Project 1. Develop a somatosensory neural interface (SSNI)

The overall goal of project 1 is to restore natural sensations of limb posture and movement through multichannel microstimulation of the normal afferent pathways involved in proprioception. Two objectives must be met to achieve this overall goal. First, we must identify an appropriate location in the somatosensory nervous system for implanting microelectrode arrays to stimulate primary afferent (PA) neurons. We are examining the somatotopic organization and recruitment of primary afferent fibers in the DRG, dorsal root, and dorsal root entry zone to develop a technique called primary afferent microstimulation (PAMS). Multichannel PAMS is used to generate a spatiotemporal pattern of sensory input that encodes limb-state information for the whole limb. Neural recordings in primary somatosensory cortex are used to evaluate the response in the brain, and evaluate the effectiveness of various inputs.

The following sub-sections provide a summary of the key results obtained over the course of this project. Briefly, we made several important advances toward the goal of creating a SSNI for restoring tactile and proprioceptive sensations after injury. First, we characterized the stimulation threshold for recruiting PA fibers (Gaunt *et al.*, 2009) and developed a computational model to provide a theoretical framework for further exploration of sensory interface design (Bourbeau *et al.*, 2011). Second, we developed an animal model for quantifying and studying how the central nervous system (CNS) responds to various patterns of sensory stimulation. These studies were performed initially in short-term experiments with anesthetized animals with the goal of evaluating the brain's response to PAMS (Hokanson *et al.*, 2011; Weber *et al.*, 2011). Results from these initial experiments have provided the basis for designing and testing stimulation paradigms that are most effective for conveying information to the brain using multichannel microstimulation in the DRG. Finally, we have developed technology and procedures for surgically implanting these electrode interfaces into animals on a permanent basis. These so-called chronic implants provide two important advantages. First, we can test the effects of stimulation in the awake animal, eliminating the effects of anesthesia on the measured responses. Second, we can examine the stability of the interface over an extended period of time. This is a crucial step in the pre-clinical assessment of this technology, which must function reliably over the full lifespan of the recipient.

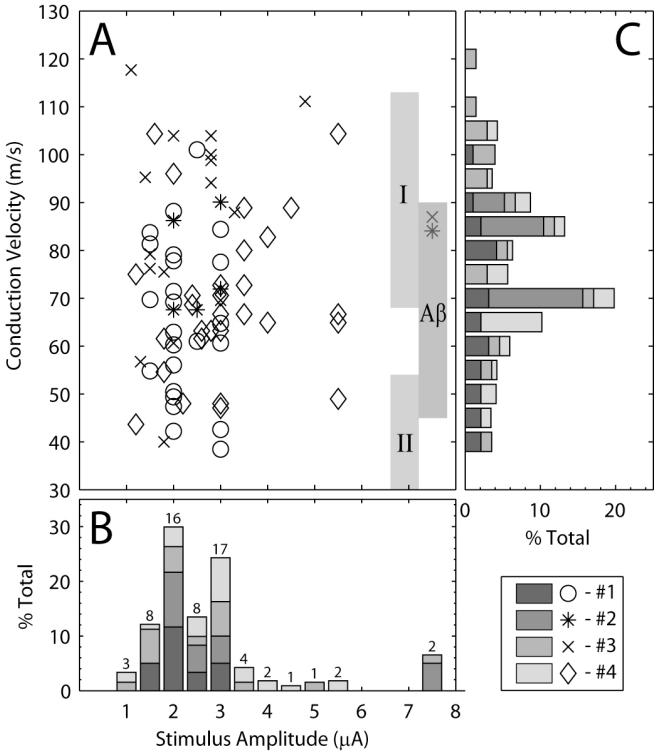

Figure 1-1: Threshold stimulus amplitudes and the CV of afferents recruited by microstimulation in the DRG. The legend identifies the data for each animal. (A) CV and stimulus amplitude for threshold responses. (B) Histogram of the threshold amplitude for all electrodes, normalized by the total number of electrodes in each animal. (C) Histogram of CVs at threshold normalized by the total number of electrodes in each animal.

Results: Recruitment of sensory fibers by microstimulation in DRG

Experiments were performed to determine the minimum current (i.e. threshold) required to excite PA neurons in the DRG and to determine the effect of

fiber diameter on the recruitment threshold. Across all cats (n=4), the threshold stimulus amplitude was 2.7 ± 1.3 μA (mean±standard deviation). The lowest stimulus amplitude that elicited a response was 1.1 μA and in 76% of the cases, the threshold stimulus amplitude was less than or equal to 3 μA. It was found that the conduction velocities (CV) of fibers recruited at threshold ranged from 38 m/s to 118 m/s, indicating that a wide range of fiber diameters can be recruited selectively at the low intensities of stimulation used in the DRG. Figure 1-1 summarizes these results in terms of the threshold stimulation amplitude and the CVs measured at threshold for each electrode. Panel A shows a scatter plot of CVs and stimulus amplitudes for all threshold responses. Panel B shows a normalized histogram of the stimulation thresholds and panel C shows a normalized histogram of the CVs of units recruited at threshold on each electrode. Two distinct peaks in the measured CVs were observed at approximately 85 m/s and 70 m/s. These correspond to the median CV of axons in the group I range (~85 m/s) and Aβ range (~72 m/s). A complete report of this study has been published (Gaunt, 2009). The key point of this figure is that PA neurons from a range of sensory modalities can be recruited at low stimulation intensities in the DRG.

Computational models have provided valuable insight into the effects of electrical stimulation on fiber recruitment in peripheral nerves. Previous models were based on specific geometries for the fiber bundles and do not generalize easily to other structures. In particular, the irregular and variable arrangement of fibers and cell bodies in the DRG make it impractical to define a specific geometry to model the various electrode-fiber configurations that are possible. An alternative approach, which has been used for modeling the recruitment of fibers by deep brain stimulation (DBS), is to estimate the volume of tissue activated (VTA) by a given stimulus current. The VTA is defined by the current-distance relation for each fiber diameter, which predicts the activation threshold as a function of the distance between the current source and nearest node of Ranvier. Thus, a given stimulus will activate all fibers having at least one node within the boundary of the VTA.

The likelihood of activating a fiber of a given diameter can be estimated by determining the probability of capturing a node of Ranvier within the VTA (see Figure 1-2). For a given fiber size, this probability depends on the internodal length as well as the probability of encountering that

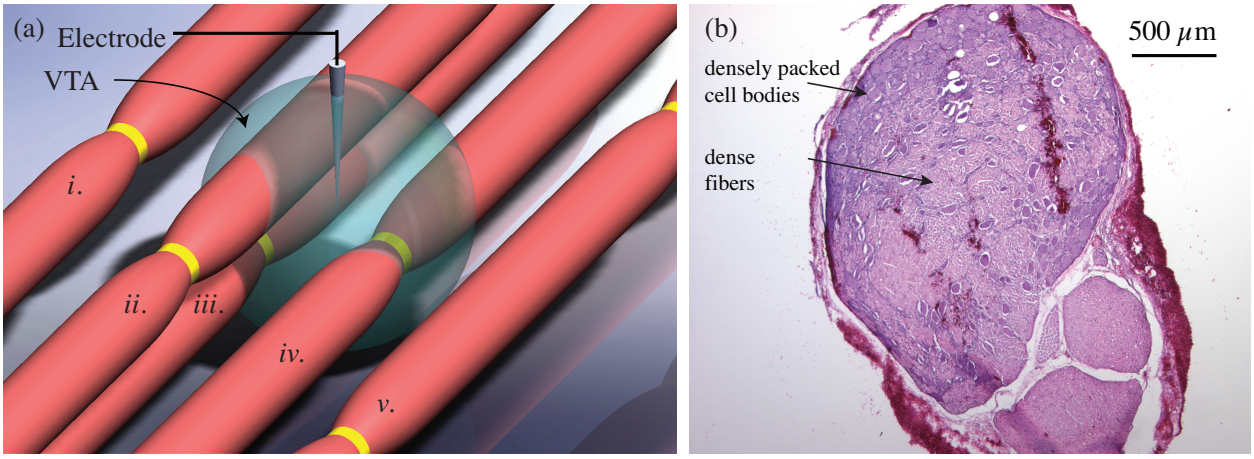

Figure 1-2: Sphere representing volume of tissue activated (VTA) by a point-source current stimulus delivered by a microelectrode. (a) The size of the sphere increases with stimulus amplitude and also varies with fiber diameter. The radius is determined by the current-distance relationship calculated with the MRG model for neuronal excitation. Fibers iii and iv, having a node of Ranvier within the VTA, will be activated. Fiber ii, though it passes through the sphere, does not have a node of Ranvier within the sphere and thus will not be activated. Fibers i and v, likewise, will not be activated. (b) Transverse section of feline L7 DRG (top) and ventral root (bottom), hematoxylin and eosin (H&E) stained. Cell bodies are predominantly located along the perimeter of the DRG, but are also sparsely distributed in the center among fibers of passage in the middle, which results in a heterogeneous tissue structure.

fiber size within the VTA. We implemented this “likelihood of activation” approach to estimate the recruitment of PA fibers by microstimulation of the DRG. This approach assumes that the distribution of fibers follows published data for the number and distribution of fibers of various diameters in the DRG. We used a multi-compartment neuron model to determine the current-distance relationship for a range of fiber diameters. Given the current-distance relationship for each fiber diameter, the model provides a likelihood estimate of the number and types of fibers recruited based on the density and distribution of fibers by size. These features lead to a flexible model that can simulate various stimulation scenarios and electrode-fiber geometries, including the inhomogeneous distribution of fibers in the DRG.

Activation of a neural fiber depends on several factors, including stimulus waveform and amplitude, fiber size, and distance from the stimulating electrode. Figure 1-3 illustrates the effect of increasing fiber diameter on the current-distance relation, which determines the size of the VTA. In general, the electrode-to-node distance increases with the stimulus amplitude. At higher intensities, the larger diameter fibers can be activated at a much greater distance, or conversely, at large distances (e.g. > 1 mm) the threshold is lower. This gives rise to the so-called ‘reverse recruitment’ phenomena that has been described for muscle activation with epineural electrodes. However, for amplitudes below 10 µA (see inset in Figure 1-3a), there is little difference in the current-distance relationship for fibers of different diameters. Thus, at these low intensities, the radius of the VTA is effectively the same for all myelinated fibers within the range tested. Although the VTA is the same for these fibers, this does not mean that these different sized fibers have equal likelihood of being recruited in the 0-10 µA range. In order for a fiber to become activated, a node of Ranvier must be captured within the VTA.

The model was used to examine the activation of medium (7.3-11.5 µm) and large (12.8+ µm) diameter PA fibers in the feline L7 DRG as a function of stimulus intensity (see Figure 1-4). Simulation results were compared to recruitment data obtained in vivo (Gaunt, Hokanson et al. 2009). Consistent with the in vivo data, the model simulations suggested that medium and large fibers have similar thresholds (~1-3 µA). However, the model simulations revealed a strong bias favoring recruitment of medium fibers, with probabilities of activation more than twice that for the large fibers. The in vivo data showed only a small bias favoring recruitment of medium fibers.

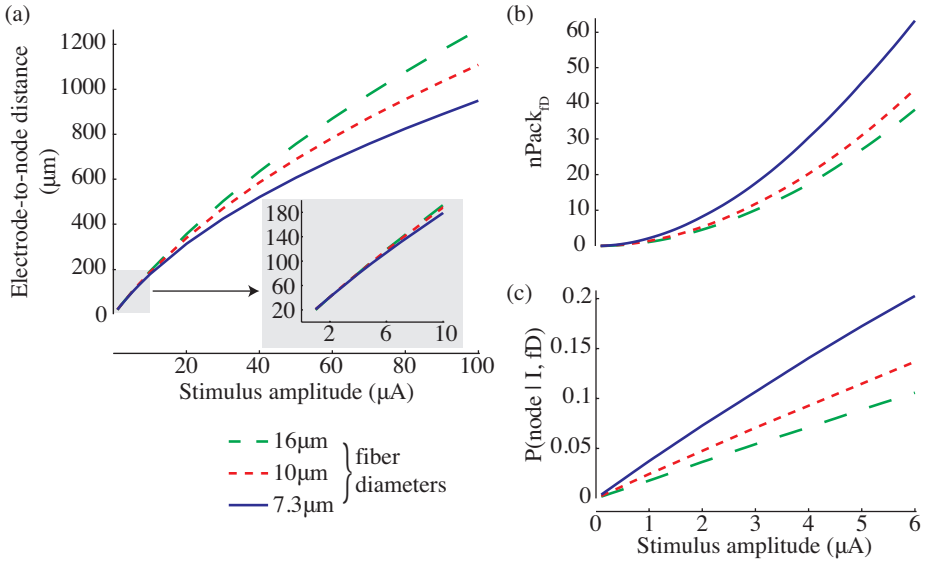

Figure 1-3: Effects of fiber diameter on current-distance relation, fiber packing and probability of having a node in the VTA. (a) Current-distance relationships from single-fiber model. Electrode-to-node distance corresponds to the radius of a spherical VTA centered about a stimulating electrode. (b) The number of fibers that can be packed into the VTA assuming a packing ratio equal to 1. (c) Probability of capturing a node of Ranvier in the VTA as predicted by (7). Fiber sizes of 7.3 µm, 10 µm and 16 µm were simulated.

Two factors contribute to this bias. First, there are approximately 55% more medium fibers than large fibers, increasing the likelihood of encountering one or more medium fibers in the VTA. Second, the internodal distance is shorter, increasing the likelihood of capturing a node of Ranvier within the VTA. The discrepancy between the simulation results and in vivo data may be due to failure to reliably detect recruitment of individual medium fibers in the in vivo study; it is likely that two or more medium fibers were actually recruited at the thresholds found for medium fibers in the in vivo study (see discussion). Finally, the model was used to estimate the number of medium and large diameter fibers recruited by stimulation currents in the range 1-6 µA, revealing a slightly sharper rate of recruitment for the medium fibers (see Figure 1-5). We conclude that this probabilistic model is useful for gaining insight into the pattern of sensory fiber recruitment by PAMS in the DRG. This information is valuable for guiding the design of microelectrode arrays for a SSNI.

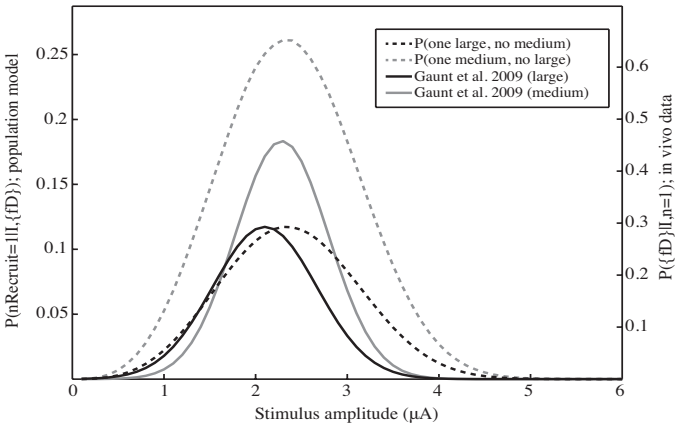

Figure 1-4: Comparison of model predictions to electrophysiology data at threshold amplitudes. The solid traces represent the probabilities of recruiting a fiber from one of the two fiber sets {fD}medium and {fD} large, given that a fiber was recruited, as a function of stimulus intensity. The dashed traces represent model predictions for recruiting a fiber from one of the two sets as a function of stimulus intensity. The gray traces represent the probabilities of recruiting exactly one large fiber (12.7-16+ µm). The black traces represent the probabilities of recruiting exactly one medium fiber (7.3-11.5 µm). The y-axis for the model data is on the left and the y-axis for the electrophysiology data is on the right (Gaunt, Hokanson et al. 2009).

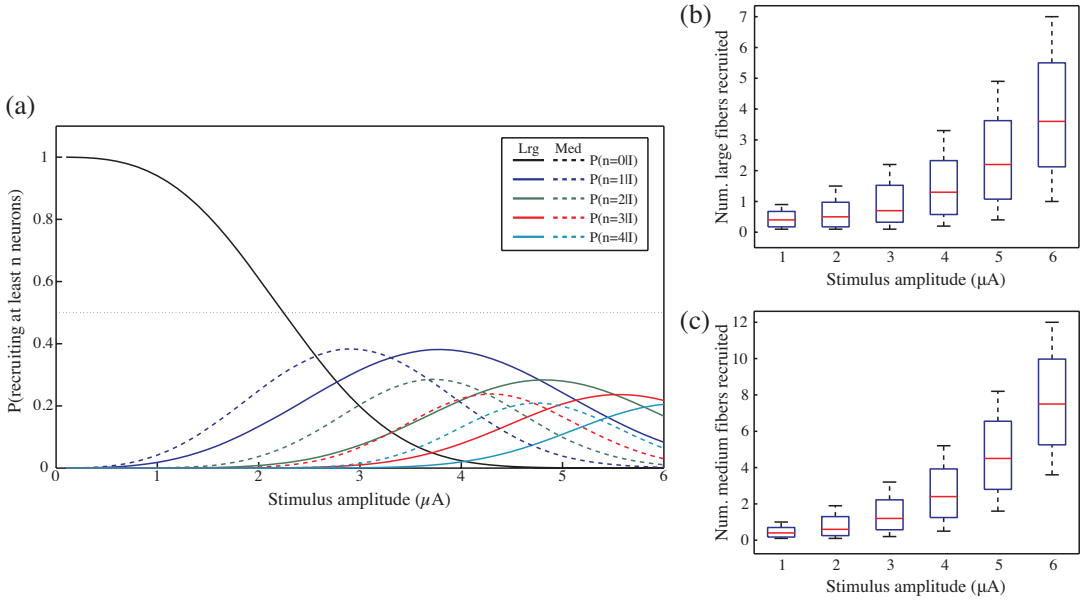

Figure 1-5: Recruitment of multiple fibers in a heterogeneous population across stimulation amplitudes in the range 1-6 µA. (a) Traces represent the probabilities of recruiting exactly zero, one, two, three, or four fibers. Solid traces represent recruitment of large fibers (12.8 to 16+ µm) while dashed traces represent recruitment of medium fibers (7.3 to 11.5 µm). (b) and (c) Range of numbers of large and medium fibers recruited, respectively, given stimulus amplitude.

Results: Quantifying the CNS response to DRG stimulation

We developed a novel animal for designing and testing a somatosensory neural interface (SSNI) for encoding and transmitting tactile and proprioceptive information by primary afferent microstimulation (PAMS) in the dorsal root ganglia (DRG). In this model, the effects of stimulation are measured in the response of a population of neurons recorded in primary somatosensory cortex (S1). Under normal conditions, the firing rates of PA neurons throughout the limb are modulated during movement, establishing a widely distributed spatiotemporal neural code representing the physical state of the limb. We have developed a 'replay stimulation' paradigm to mimic the global pattern of PA activity produced during movement. Admittedly, the replay pattern is not an exact recreation of the normal PA input, since only a subset (n <= 32 stimulation channels) of the total PA population is activated and may include additional fibers than the ones recorded. By comparing S1 responses to passive movement and replay PAMS, we can gain insight into the amount of movement-related information received in the brain in response to the movement and replay conditions. Further, we can systematically alter the structure (e.g. number and ordering of channels) of replay inputs to examine the effects on S1 responses.

Recordings were made simultaneously in the DRGs and S1 during displacements of the hindpaw. Next, recordings were made in S1 during PAMS (7 and 10 µA) on 30 DRG channels. PAMS pulse patterns on each DRG channel were set to match the spike times recorded during movement trials (i.e. replay PAMS). Extra pulses were inserted on some trials to increase the pulse rate to 4x and 8x the original rate (see Figure 1-6). S1 firing rates were highly correlated with foot speed during movement trials. Linear regression was used to estimate foot speed from firing rates on these 48 channels (R2 = 0.96). Similar models were used to estimate foot speed in replay trials (R2 = 0.40 at the base rate and 7µA). Increasing the replay rate to 4x enhanced the cortical response, yielding a stronger estimate of foot speed (R2 = 0.64), but 8x replay yielded a weaker S1 response (R2 = 0.43). This trend was also observed at 10 µA with R2 values of 0.60, 0.76, and 0.58 for 1x, 4x, and 8x respectively.

These results show that PAMS with only 30 channels is effective at evoking neural responses in S1 that are similar to those evoked by whole limb movement. Further, amplifying the stimulation pulse rate can enhance the

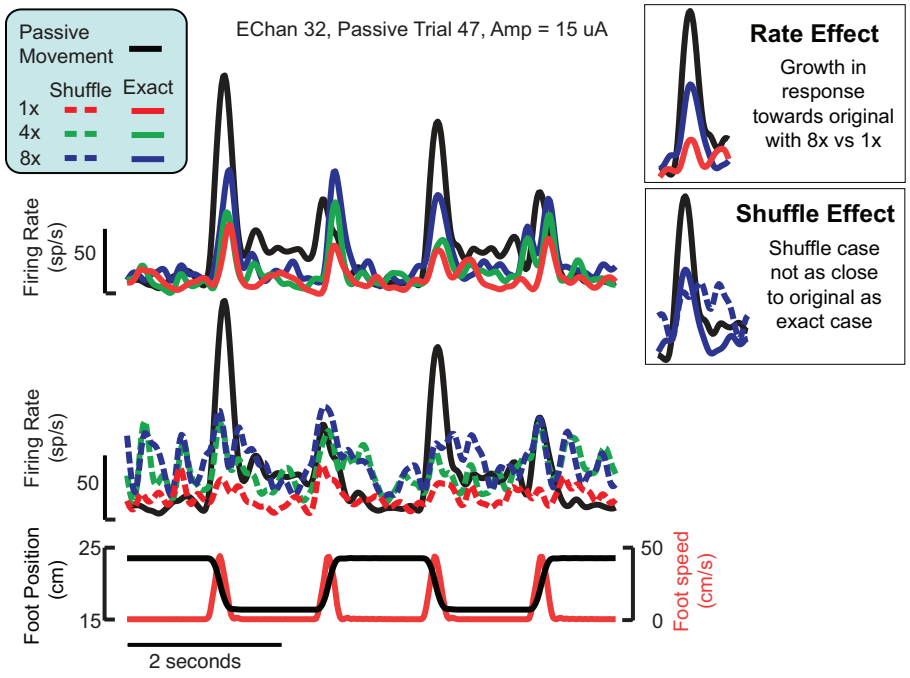

Figure 1-6: Stimulation pulse rate and channel shuffle effects. The example shows the cortical response (firing rate) of a single channel to passive movement and 1x, 4x, and 8x replay stimulation rates (top) and channel shuffles (below). Increasing the stimulus pulse-rate shows an increased cortical response during the exact match case.By shuffling stimulus channels the signal degrades, showing that the response is not merely a result of the aggregate stimulation rate.

cortical response, but the range of pulse rates may be limited. By using higher than normal pulse rates, we hypothesize that temporal summation at downstream synapses may partially compensate for the limited number of input channels. The use of replay stimulation and its variants provide a basis for examining the use of PAMS in providing proprioceptive feedback.

We also tested several simple patterns of PAMS to examine the sensitivity of the S1 neuronal response to variations in the intensity, pulse-rate, and location of stimuli applied in the DRG. These experiments are important for designing sensory stimulation patterns that are effective in conveying detectable and discriminable information to the brain. S1 neural responses were used as inputs to a Naïve Bayes Classifier. Figure 1-7A shows classification accuracies for stimulation patterns that varied in amplitude (5 levels between 3 and 20 μA) and location (5 different electrode pairs); the pulse-rate was fixed at 20 pps for panels A and B.

Four input locations (columns 1,2, 4, and 5 in figure 1-7A) evoked S1 responses that could be detected from the background discharge with high reliability (>90%), even at intensities as low as 3 μA. Accurate discrimination between the effects of two adjacent stimulus locations was also possible (panel B). Interestingly, panel B shows a non-monotonic relationship between classification accuracy and stimulation amplitude – intensities above 11.5 μA and below 7.2 μA had lower classification accuracies. Thus, while high-intensity stimulation may evoke stronger responses in S1, the ability to distinguish different input locations, particularly ones adjacent to each other as in (B), may degrade at higher stimulation intensities. This degradation may be due to the recruitment of larger and potentially nonhomogeneous populations of afferent neurons resulting in less discriminable patterns of activity in S1.

We also examined the effect of varying the stimulus pulse-rate. The matrix plot in figure 1-7C shows the classification accuracies for discriminating pairs of stimuli having different pulse-rates, with the amplitude fixed at 6 μA and stimulating on all 16 DRG channels. The top, left square in this matrix shows that the S1 responses to 200 pps could be distinguished with high accuracy from those evoked by 1000 pps stimuli with high accuracy. In general, stimulation frequency differences greater than 400 pps were clearly distinguishable even up to rates of 1000 pps. The inset in panel C shows an example of the multiunit response to stimulation at these frequencies. These results indicate that fabricated patterns of PAMS elicited responses in S1 that were broadly responsive and sensitive to variations in the stimulus pulse-rate, even those well beyond the normal physiological range for DRG neuron spike rates.

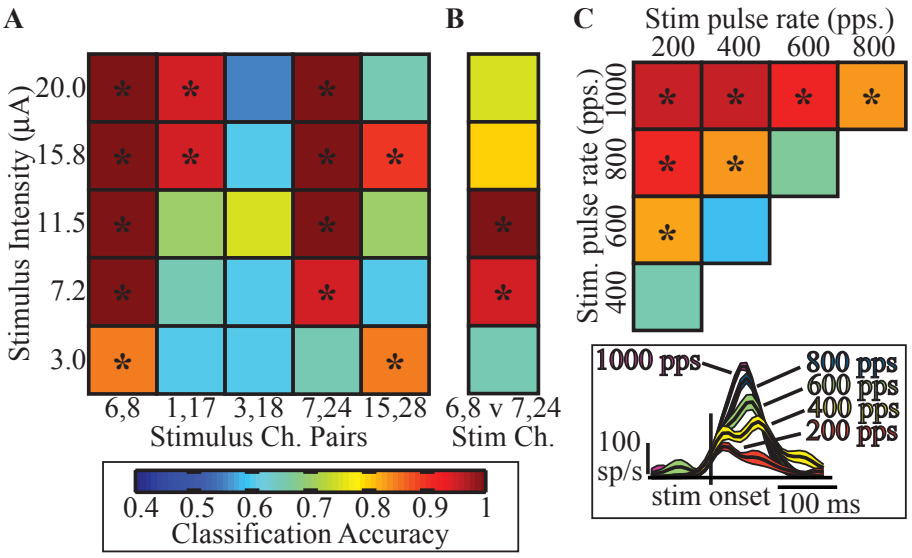

Figure 1-7: Discriminability of S1 neuronal responses to fabricated patterns of PAMS in cats. (A) S1 LFP response detection accuracy for PAMS of 5 different amplitudes (rows), applied to different DRG electrode locations represented by pairs of active electrodes (columns) and (B) classification accuracy of the effects of two stimulation locations (cat 3). (C) Classification accuracy between S1 firing rate responses to different stimulation pulse-rates (synchronous stimulation on all 16 DRG electrodes, amplitude = 6 μA; cat 2). The color scale for classification accuracy is shown at the bottom left. The inset shows examples of PSTH plots for one S1 channel for a range of stimulation pulse-rates; plots show the mean +/- 1SEM firing rates. Asterisks indicate significance ($p<0.001$).

Results: Quantifying the effects of DRG microstimulation using chronically implanted electrodes

Our initial experiments were performed in anesthetized cats during acute experiments. Results from these experiments demonstrated that varying patterns of PAMS evoke discriminable responses in S1 cortex. However, performing these experiments acutely poses several changes that may be overcome by transitioning to a chronic implant model. First, the number of well isolated cortical units generally peaks several weeks after surgery. Performing an acute experiment requires that staff must operate for multiple days with limited sleep increasing the potential for mistakes. Time limitations preclude detailed analysis between trials that might inform the ongoing procedure. Evoked sensory responses are very much anesthesia dependent and switching drugs is typically not an option in a terminal surgery. Finally, acute experiments preclude the possibility of gathering any behavioral data collected during DRG stimulation.

Chronic cortical recording studies were performed in a cat both while awake and while under anesthesia. Protocols were approved by the University of Pittsburgh IACUC. Isoflurane (1-2%) was used to anesthetize the cat during a craniotomy performed in a sterile surgical field. A 96-channel penetrating electrode array (Utah MEA, Blackrock Microsystems) was implanted in the hindlimb area of S1 cortex (post-cruciate gyrus) with lead wires routed under the skin to a Cereport connector. Both reference wires were placed epidurally and during recording sessions were shorted using external jumpers. The animal was monitored for several days post-surgery and recording experiments began 5 days after surgery.

Initial recordings were performed with the animal anesthetized using either isoflurane or medetomidine to evaluate the quality of recordings under each. A gross channel identification procedure was performed using isolated movements of individual joints or skin palpation. Transcutaneous electrical stimulation was applied to several locations on both limbs as well. Signals were captured at 25 kHz using an RZ2 system (TDT). Prior to cortical implantation surgery the cat was trained daily to maintain quiet stance and to walk on a split belt treadmill (Bertec). After a post-surgery recovery period, training continued with routine recording sessions on alternate days.

During walking, ground reaction forces were recorded and digitized at 1 kHz from force plates located beneath each belt of the treadmill. Motion capture data and video was recorded at 100 Hz from 12 cameras (OptiTrack, NaturalPoint). A multichannel recording system (Grapevine, Ripple) system was used to capture neural spiking data at 30 kHz. Spike events were created from thresholded waveforms and sorted into isolated units (Offline Sorter, Plexon).

Coarse unit identification was performed using a variety of methods, but transcutaneous stimulation under medetomidine proved to be the most informative. Of all 96 channels 21 responded to forelimb (elbow) stimulation, 12 responded to hindlimb (knee), and 7 responded to both (t-test; $p < .01$). Hindlimb channels were located medially and forelimb laterally in rough agreement with the expected somatotopic organization of the post-cruciate gyrus.

Early results from treadmill walking (Figure 1-8) have validated successful array implantation and high quality unit recordings were captured on multiple channels. On average each channel recorded 1.4 +/- 0.6 units. Phasic activity roughly aligned with walking was present on a subset of channels. Further development of motion capture system interoperability is required to establish accurate step timing to average

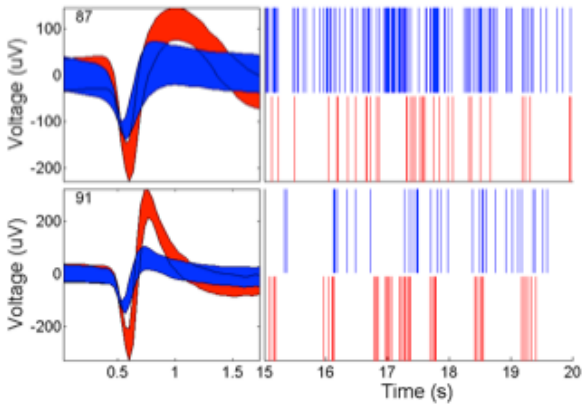

Figure 1-8: Phasic modulation in S1 cortical activity recorded during treadmill locomotion.

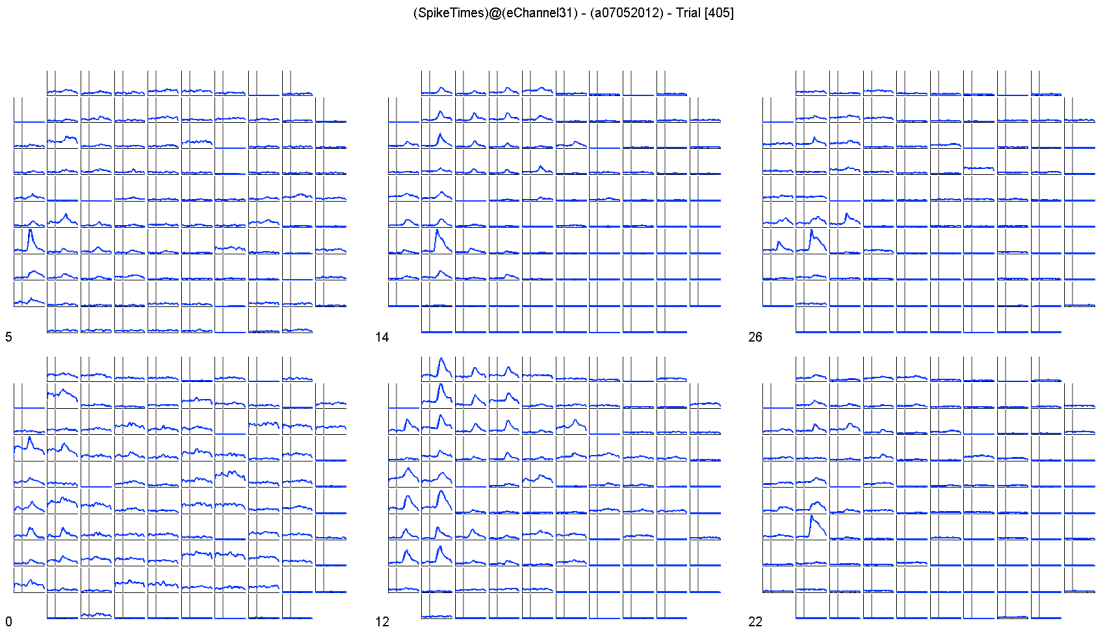

Figure 1-9: Chronic stability of evoked neural responses in S1. Each plot shows a map of the evoked responses (peristimulus time histograms, PSTH) across the 96 channel array. The number of days is listed at the bottom left of each plot (day 0 to day 26).

responses during walking.

Initial recording sessions have demonstrated the feasibility of chronically implanting an electrode array in S1 cortex to record evoked neural activity over time. Longitudinal studies of DRG microstimulation are needed to determine the viability of the DRG as a viable substrate for future neural prosthetics. These studies will allow testing of DRG stimulation model stability across many days.

Figure 1-8 shows the peristimulus time histograms (PSTHs) for responses evoked by microstimulation (10 μA, 600 pulses @ 1 pulse/sec) on a single channel in the L7 DRG across 26 days of testing. Each plot shows PSTHs for 96 electrodes mapped according to their spatial layout in the S1 array. The vertical scale for each PSTH is normalized to the maximum firing rate measured for each day. It is clear that the 10 uA stimulus evokes a pattern of responses in S1 that is very consistent from day 5 and beyond. These results are encouraging in demonstrating the reliability of the brain's response to DRG microstimulation over approximately one month of testing.

Reportable outcomes for work relevant to Project 1

Journal papers

Bourbeau DJ, Hokanson JA, Rubin JE & Weber DJ (2011). A computational model for estimating recruitment of primary afferent fibers by intraneural stimulation in the dorsal root ganglia. *J Neural Eng* **8,** 056009.

Bruns TM, Gaunt RA & Weber DJ (2011*a*). Multielectrode array recordings of bladder and perineal primary afferent activity from the sacral dorsal root ganglia. *J Neural Eng* **8,** 056010.

Wagenaar JB, Ventura V & Weber DJ (2011). State-space decoding of primary afferent neuron firing rates. *J Neural Eng* **8,** 016002.

Wang W, Collinger JL, Perez MA, Tyler-Kabara EC, Cohen LG, Birbaumer N, Brose SW, Schwartz AB, Boninger ML & Weber DJ (2010*a*). Neural interface technology for rehabilitation: exploiting and promoting neuroplasticity. *Phys Med Rehabil Clin N Am* **21,** 157–178.

Weber DJ, London BM, Hokanson JA, Ayers CA, Gaunt RA, Torres RR, Zaaimi B & Miller LE (2011). Limb-state information encoded by peripheral and central somatosensory neurons: implications for an afferent interface. *IEEE Trans Neural Syst Rehabil Eng* **19,** 501–513.

X Miller LE, Weber DJ (2011). Brain training: cortical plasticity and afferent feedback in brain-machine interface systems. IEEE Trans Neural Syst Rehabil Eng. 19(5): 5 pp. PMID: 21947530

Conference papers

Bruns TM, Gaunt RA & Weber DJ (2011*b*). Estimating bladder pressure from sacral dorsal root ganglia recordings. *Conf Proc IEEE Eng Med Biol Soc* **2011,** 4239–4242.

Gaunt RA, Hokanson JA & Weber DJ (2009). Microstimulation of primary afferent neurons in the L7 dorsal root ganglia using multielectrode arrays in anesthetized cats: thresholds and recruitment properties. *J Neural Eng* **6,** 055009.

Collinger JL, Dicianno BE, Weber DJ, Cui XT, Wang W, Brienza DM & Boninger ML (2011). Integrating rehabilitation engineering technology with biologics. *PM R* **3,** S148–S157.

Rigosa J, Weber DJ, Prochazka A, Stein RB & Micera S (2011). Neuro-fuzzy decoding of sensory information from ensembles of simultaneously recorded dorsal root ganglion neurons for functional electrical stimulation applications. *J Neural Eng* **8,** 046019.

Gaunt RA, Bruns TM, Crammond DJ, Tomycz ND, Moossy JJ & Weber DJ (2011). Single- and multi-unit activity recorded from the surface of the dorsal root ganglia with non-penetrating electrode arrays. *Conf Proc IEEE Eng Med Biol Soc* **2011,** 6713–6716.

Hokanson JA, Ayers CA, Gaunt RA, Bruns TM & Weber DJ (2011). Effects of spatial and temporal parameters of primary afferent microstimulation on neural responses evoked in primary somatosensory cortex of an anesthetized cat. *Conf Proc IEEE Eng Med Biol Soc* **2011,** 7533–7536.

Abstracts

Bourbeau DJ, Hokanson JA, and Weber DJ. A computational model for selectively stimulating peripheral sensory neurons. In: Society for Neuroscience Annual Meeting. San Diego, CA: 2007, p. 728.711.

Hokanson JA, Wagenaar JB, and Weber DJ. Neuronal responses in somatosensory cortex to multichannel microstimulation of primary afferent neurons. In: Society for Neuroscience Annual Meeting. San Diego, CA: 2007, p. 728.710.

Wagenaar JB, Sudre G, Ventura V, and Weber DJ. Quantifying somatosensory neuronal responses using conditional mutual information. In: Society for Neuroscience Annual Meeting. San Diego, CA: 2007, p. 728.712.

Weber DJ, Hokanson JA, and Wagenaar JB. Providing somatosensory feedback via multichannel microstimulation of primary afferent neurons. In: BMES Annual Fall Meeting. Los Angeles, CA: 2007.

Bourbeau DJ, Hokanson J, Weber DJ. (2008). A computational model for examining activation of peripheral neurons by electrical microstimulation. In BMES 2008 Annual Fall Meeting. St. Louis, MO.

Hokanson J, Wagenaar JB, Weber DJ. (2008a). Recruitment of DRG neurons by electrical microstimulation. In BMES 2008 Annual Fall Meeting. St. Louis, MO.

Hokanson JA, Wagenaar JBW, Weber DJ. (2008b). Recruitment of DRG neurons by electrical microstimulation. In Society for Neuroscience Annual Meeting, pp. 779.715. Washington, DC.

Wagenaar J, Ventura V, Weber DJ. (2008a). Limb State Estimation from afferent cell-responses; Inverse model estimation using particle filtering. In Society for Neuroscience Annual Meeting, pp. 779.714. Washington, DC.

Wagenaar JB, Hokanson J, Ventura V, Weber DJ. (2008b). Real-time feedback control of functional electrical stimulation based on primary afferent recordings. In BMES 2008 Annual Fall Meeting. St. Louis, MO.

Bourbeau DJ, Weber DJ. (2009). Hindlimb Endpoint Forces Evoked by Microstimulation of Ventral Root Nerves in Rat. In BMES 2009, pp. PS-9A-113. Pittsburgh, PA.

Hokanson JA, Weber DJ. (2009). Using Classifiers to Identify Differences in Evoked Responses from Stimulation of Primary Afferents In BMES 2009, pp. OP-10-11-18B. Pittsburgh, PA.

Perich MG, Hokanson JA, Gaunt RA, Weber DJ. (2009). Improving Limb-State Decoding Using a Liquid State Machine In BMES 2009. PS-9A-168, Pittsburgh, PA.

Wagenaar JB, Gaunt RA, Ventura V, Weber DJ. (2009a). Feedback Control of FES by Online Decoding of Limb-Position from the Firing Rates of Muscle and In BMES 2009, pp. OP-9-1-7A. Pittsburgh, PA.

Wagenaar JB, Ventura V, Weber DJ. (2009c). Improved decoding of limb-state using feedback from natural sensors. In Society for Neuroscience Annual Meeting, pp. 175.111/Z138 Chicago, IL.

Weber DJ, Loeb G, Francis JT, Schwartz AB. (2009a). Sensable Neuroprosthetics. In Winter Conference on Brain Research. Copper Mountain, CO.

Ayers CA, Gaunt RA, Hokanson JA, Weber DJ (2010) Primary somatosensory cortex responses to simple patterns of primary afferent microstimulation in L6/L7 dorsal root ganglia of anesthetized cats. Program No 29515 2010 Neuroscience Meeting Planner San Diego, CA: Society for Neuroscience, 2010 Online.

Bourbeau DJ, Hokanson JA, Rubin JE, Ermentrout GB, Weber DJ (2010) A computational model for simulating recruitment of peripheral nerve fibers by intraneural microstimulation. Program No 38314 2010 Neuroscience Meeting Planner San Diego, CA: Society for Neuroscience, 2010 Online

Bruns TM, Gaunt RA, Simpson TW, Weber DJ (2010) Primary afferent neural activity recorded with non-penetrating electrodes on lumbar DRG surface. Program No 29516 2010 Neuroscience Meeting Planner San Diego, CA: Society for Neuroscience, 2010 Online.

Hokanson JA, Ayers CA, Gaunt RA, Weber DJ (2010) Novel stimulation paradigm to provide somatosensory feedback in a neural prosthesis. Program No 29512 2010 Neuroscience Meeting Planner San Diego, CA: Society for Neuroscience, 2010 Online

Wagenaar JB, Hokanson JA, Ayers CA, Weber DJ (2010) Development of an efficient data-management system in Matlab. Program No 20912 2010 Neuroscience Meeting Planner San Diego, CA: Society for Neuroscience, 2010 Online

Bruns TM, Gaunt RA & Weber DJ (2011). Sacral dorsal root ganglia recordings of bladder and perineal sensory activity. In Society for Neuroscience Annual Meeting, p. 711.11.

Gaunt RA, Bruns TM & Weber DJ (2011). Microstimulation of sacral dorsal root ganglia for reflex bladder control. In Society for Neuroscience Annual Meeting, p. 711.12.

Patent applications

D.J. Weber, R.A. Gaunt, T.M. Bruns, Apparatus and method for monitoring and regulating physiological functions via sensory neural inputs to the spinal cord. Provisional application filed March 20, 2012.

Project 2. **Establishment of neural interface stability and optimization**

The implanted neural interface must remain stable throughout the lifespan of the user, but immune and inflammatory reactions at the implant site are known to degrade the performance of implanted microelectrodes. Since tissue reactions vary in different parts of the nervous system, our objectives are 1) to examine the tissue responses around electrodes implanted in the DRG and spinal cord 2) to test whether surface coating, with agents that encourage specific neuronal survival and growth and reduce inflammation, will be effective in improving the biocompatibility and 3) to examine the effect of chronic stimulation on surrounding tissue. In the first two years of the project, we have optimized the probe implantation, tissue processing and quantification protocols, developed neuron promoting L1 coating and electrically controlled dexamethasone release coatings. In the past year, we have completed the chronic implantation and histology study. Extensive characterization of the cellular tissue response around the electrodes in DRG and SC at both acute and chronic time points was performed. The effect of the L1 coating was evaluated in vivo, and encouragingly the L1 coating showed trends of reduced microglia/macrophage activation and kill zone size. A novel PEDOT/carbon nanotube coating was developed for the stimulating electrodes. This coating can be directly deposited on the electrode sites and improve the impedance and charge injection capacity of the electrodes by several orders. Such properties are expected to induce less tissue damage caused by chronic stimulation. In addition, anti-inflammatory drug can be released during the stimulation to further protect the neurons and reduce scarring. Below is detailed report on these results.

Result 1: *Characterization of the tissue responses around neural electrodes in DRG and spinal cord on uncoated and L1 coated probes*

This work has been published in the June 29th issue of *Acta Biomaterialia* (reference listed in reportable outcomes).

Result 2: *Development and characterization of PEDOT/carbon nanotube (CNT) coating*

The *in vitro* characterization of the coating has been completed and published in Biomaterials. The Dexamethasone containing PEDOT/CNT coating has been applied to in vivo microwire arrays and tested in chronic stimulation as reported in Result 3.

Results 3: *Characterization of electrode performance and tissue response to chronically stimulated microelectrodes implanted into the dorsal root ganglion*

The purpose of this study was to evaluate the effects of chronic stimulation on electrode performance and tissue response in the dorsal root ganglion (DRG). Three coating conditions were evaluated including no coating (NC), PEDOT/carbon nanotube (CNT) coating and PEDOT/CNT/Dexamethasone (PCD) coating. We are currently editing a manuscript draft of this work for submission to the Journal of Neural Engineering in early September. However, our results are summarized below.

To further investigate the DRG as a potential site for neural recording and stimulation, we implanted dual microelectrodes into adult rats and subjected animals to a daily stimulation regimen over a two-week time period. For these studies, electrodes were implanted into the DRG at either L6 or L7 with lead wires connected to an adaptor on the skull of the animal allowing for chronic stimulation (animals in each group outlined in Table 2-1). The paradigm utilized was based on that used previously in the cerebral cortex of the cat [1] and an overview of our approach is provided in Figure 2-1.

Following fabrication of the dual microelectrodes, one of two modifications was made to the electrode surface. For both the PC-coated (Figure 2-2B) and PCD-coated (Figure 2-2C) electrodes, we observed a generally uniform distribution of CNTs. The surfaces were rougher and more porous than the non-coated (NC) controls (Figure 2-2A). With the PC coating, a lower *in vitro* impedance value was observed in comparison to the NC and PCD-coated electrodes (Figure 2-3A). *In vitro* studies were also used to evaluate the amount of dexamethasone released as a function of the number of stimulations. When stimulated alongside implanted animals, drug release was observed for each of the four stimulations performed indicating sustained dexamethasone release over time (Figure 2-3B).

To evaluate electrode performance, a number of measures were taken for both non-stimulated and stimulated electrodes. First we compared the effect of stimulation on the impedance (Z) value at 1 kHz by combining all coating conditions. With stimulation, the Z values were lower than without stimulation (Figure 2-4A; $p < 0.001$). We then evaluated potential changes in Z over time by coating condition. Without stimulation, there were no statistically significant changes in Z for any of the coating conditions (data not shown). In addition, there were no significant differences in Z between the three coating conditions (data not shown). However, with stimulation, the Z for PC-coated (Figure 2-4B; $p < 0.05$ for days 1-3) and PCD-coated electrodes (Figure 2-4B; $p < 0.05$ for days 1-3 and days 4-7) were significantly lower than the Z for NC electrodes. The more prolonged lowering of the Z for the PCD-coating may be a result of the repeated release of dexamethasone which could reduce tissue inflammation and indirectly influence Z values.

We then evaluated the correlation between Z and electrode potential (both positive and negative) to ensure that our stimulation and Z measures were valid (Figure 2-4C). The results of Pearson correlation tests indicate that Z values correlate with both + potential ($p < 0.001$; $R^2 = 0.4323$) and – potential ($p < 0.001$; $R^2 = 0.5604$). This correlation underscores the benefit of lower Z values. That is, lower electrode potentials are safer for both the tissue and the implanted electrode.

Finally, cyclic voltammetry (CV) and cathodic charge storage capacity (CSC) measures were obtained and compared across coating conditions (Figure 2-5). CV measurements were made at 50 mV/s between potential limits of -0.6 V and 0.8 V. These CVs were then used to determine the CSC by calculating the time integral of the negative current during a full CV cycle. The CSC of all three electrode coatings increased as a function of time; this increase appears approximately linear with time for each of the three coating conditions. However, the increase in CSC for the PCD-coated electrodes had the steepest slope as compared to both the NC and PC-coated electrodes.

We performed a number of histological stains to evaluate and characterize the tissue reaction in response to the NC, PC-coated and PCD-coated electrodes (antibodies outlined in Table 2-2). First, to determine the degree of neuronal and axonal loss around the implant site, NF200 was used. NF200 staining was decreased or absent in the area immediately surrounding the implant site (Figure 2-6).

We also sought to characterize some of the non-neuronal cellular response including the reactions associated with microglia/macrophages and fibroblasts using Iba1 and vimentin antibodies, respectively. Cells that stained positive for Iba1 were localized to the area immediately surrounding the implant, and Iba1 intensity decreased as a function of distance from this interface (Figure 2-6). The staining intensity was highest at the site of the implant and

decreased further from this interface. Regardless of the coating condition, the Iba1 intensity increased initially and then declined to reach a background level further from the interface. Peak Iba1 intensity occurred at approximately 55.0 μm, 85.0 μm and 65.0 μm for NC, PC-coated and PCD-coated electrodes, respectively.

Vimentin immunoreactivity was relatively homogenous throughout the tissue indicating that the implanted electrode and chronic stimulation do not elicit a pronounced effect on vimentin-positive cells (including endothelial cells and fibroblasts) (Figure 2-7). Staining for the transmembrane cell surface glycoprotein, L1 was observed at the electrode-tissue interface (Figure 2-7). Increased L1 immunoreactivity was observed around the interface with background levels found further from this interface.

Finally, to determine the impact on neuronal cell death, the colocalization of NeuN and activated caspase-3 was determined (example images provided in Figure 2-8). Both PC-coated and PCD-coated electrodes were associated with a decrease in the percentage of neuronal cell death as assessed by the number of NeuN/caspase-3 positive cells versus NeuN positive cells as compared to the NC controls (Table 2-3).

Table 2-1. Overview of Animals Used for Chronic Stimulation

Coating Condition	Number of Animals	Electrodes Evaluated	Stimulation (Y/N)
NC	2	3	N
PC	3	6	Y
PCD	1	2	N
NC	3	6	Y
PC	2	2	N
PCD	3	6	Y

Table 2-2. Antibodies used for histological characterization

Antibody	Specificity
NF200	Mature axons
Iba1	Microglia/macrophages
L1	Neural cell adhesion molecule
Vimentin	Immature and reactive astrocytes, microglia, endothelial cells, fibroblasts
NeuN	Neuronal nuclei
Caspase-3	Cleaved (activated) caspase-3

Table 2-3. NeuN/Caspase-3 colocalization

Coating Condition	Stimulation (Y/N)	Percentage of NeuN/Caspase-3 Positive Cells
NC	N	54.5% (73 of 134)
	Y	51.9% (204 of 393)
PC	N	15.1% (25 of 166)
	Y	19.7% (27 of 137)
PCD	N	14.2% (47 of 331)
	Y	14.1% (22 of 156)

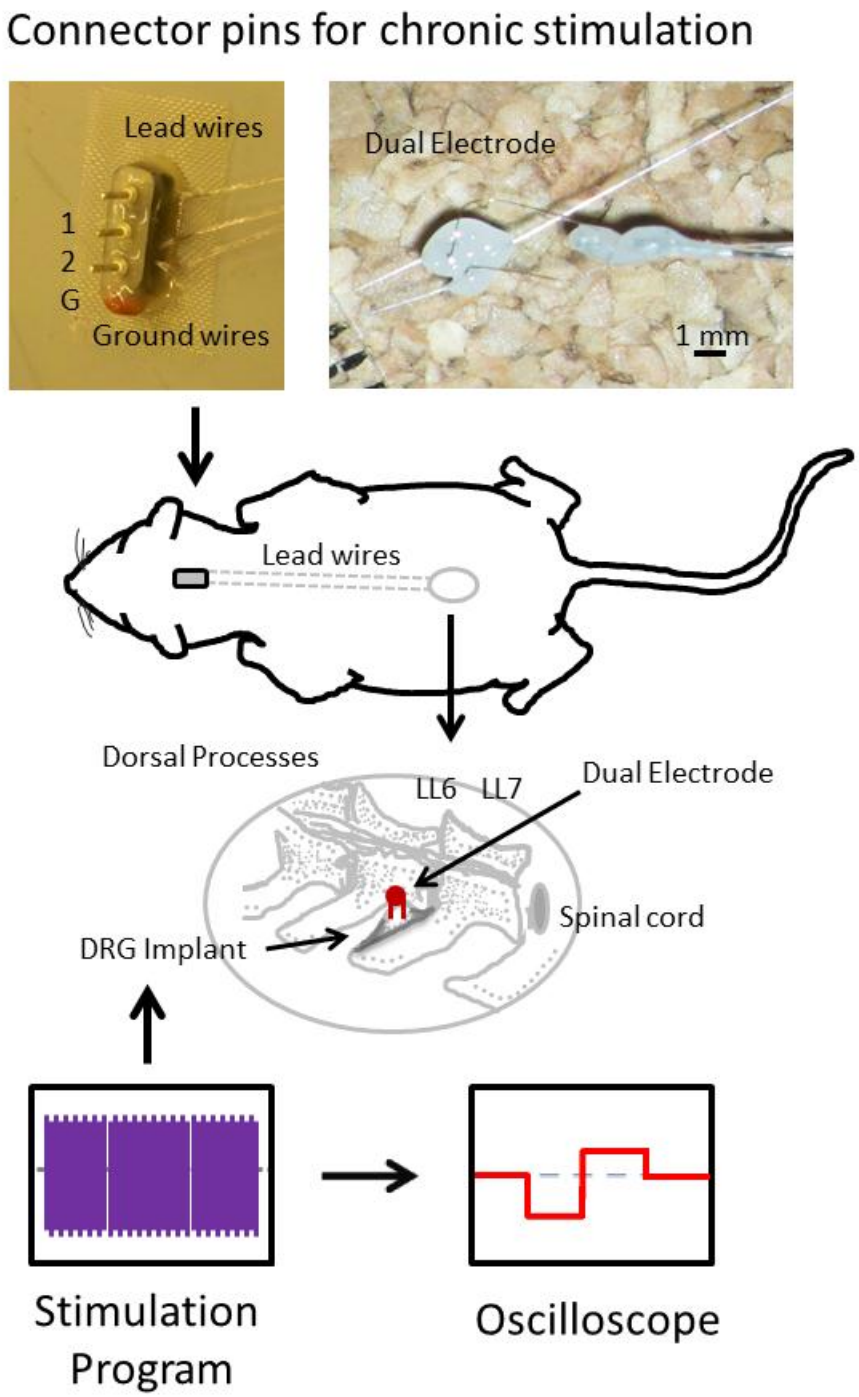

Figure 2-1. Diagrammatic overview of the chronic stimulation surgery. Dual electrodes were implanted into the DRG at L6 or L7. Lead wires ran from the electrodes up the back of the animal to an adaptor affixed to the skull. This head fixture allowed for chronic stimulation and included ground, electrode 1 (1) and electrode 2 (2) connections. Animals were subjected to 10 days of 400 µs pulses at 20 µAmps at 200 Hz for 1 hour/day and the stimulation paradigm monitored with an oscilloscope.

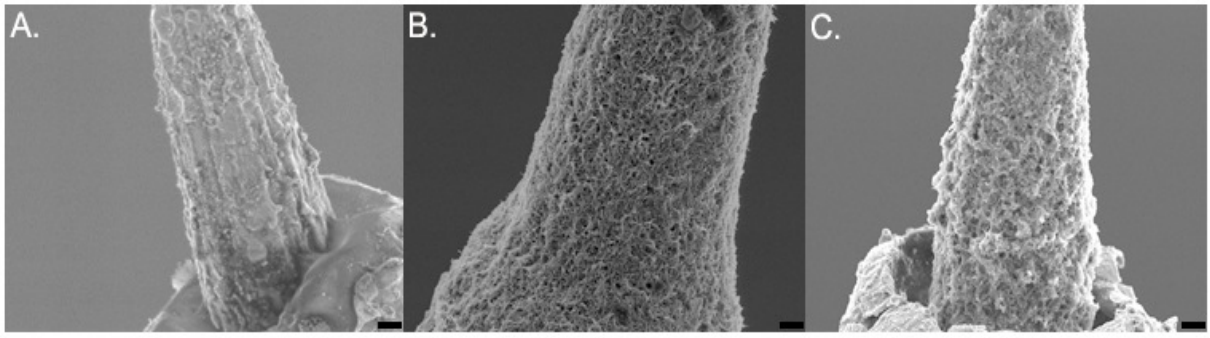

Figure 2-2. Electrode coatings. Scanning electron micrograph (SEM) images of NC (A), PC (B) and PCD (C) electrodes. Scale bar represents 1 μm.

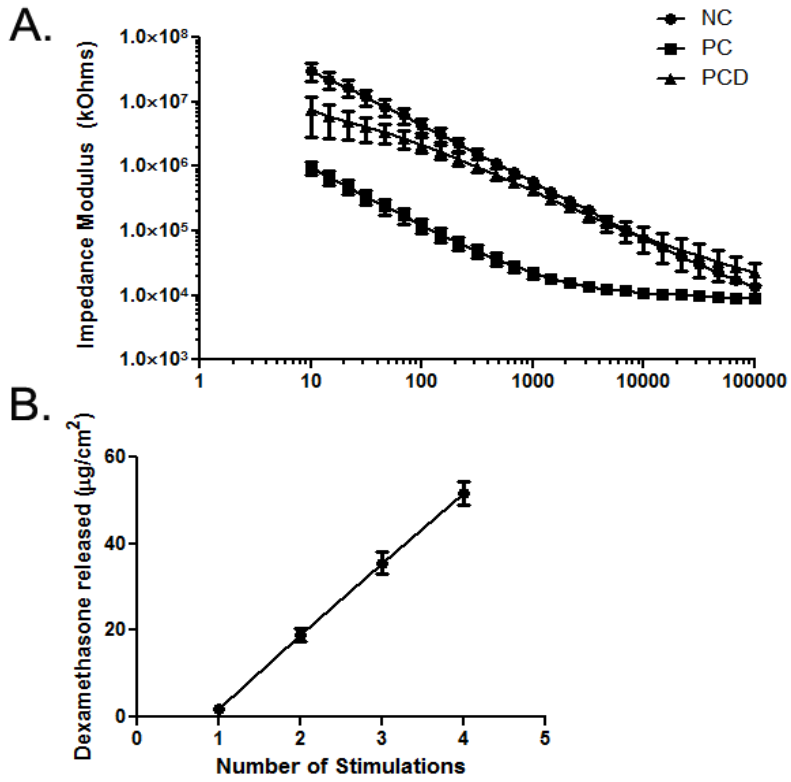

Figure 2-3. **A**: *In vitro* electrical impedance (Z) spectroscopy for each coating condition. The lowest Z values were observed with the PC coating (solid squares) and incorporation of dexamethasone resulted in an impedance spectrum for the PCD coating (solid triangles) similar to that observed with NC (solid circles). **B**: PCD-coated electrodes were subjected to the stimulation parameters utilized for *in vivo* studies (alongside anesthetized animals) and the amount of dexamethasone release quantified across these stimulations.

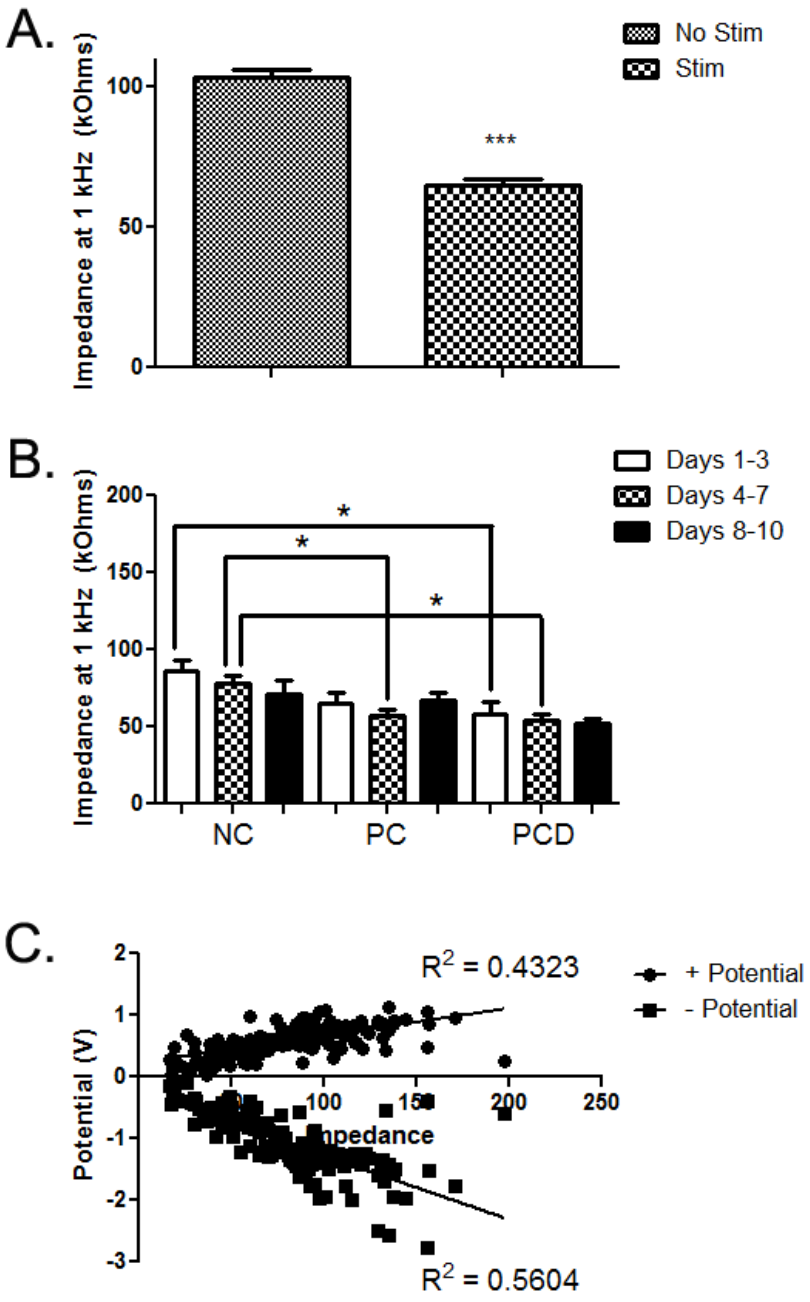

Figure 2-4. Electrode impedance (Z) at 1 kHz. **A**: With stimulation, lower Z was observed at 1 kHz when all coating conditions were combined. **B**: Impedance values at 1 kHz were grouped based on coating condition and day of stimulation. Statistically significant decreases in Z were observed with the PC coating (4-7 days) and with the PCD coating (1-3 and 4-7 days) when compared to NC controls. C: Correlation between impedance and + potential and – potential. *p < 0.05: ***p < 0.001

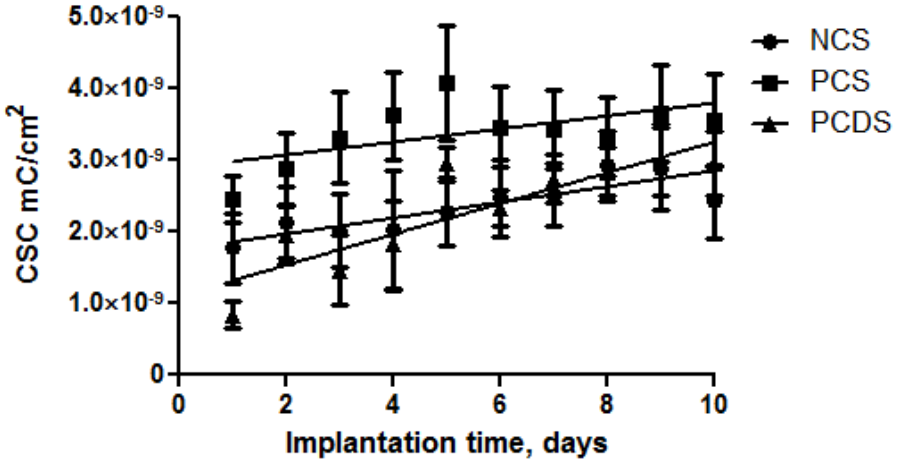

Figure 2-5. Electrical performance of implanted electrodes. Cathodal charge storage capacity (CSC) was measured at 50 mV/s and averaged over the total number of implanted electrodes for each coating condition as a function of time. Error bars represent standard error mean.

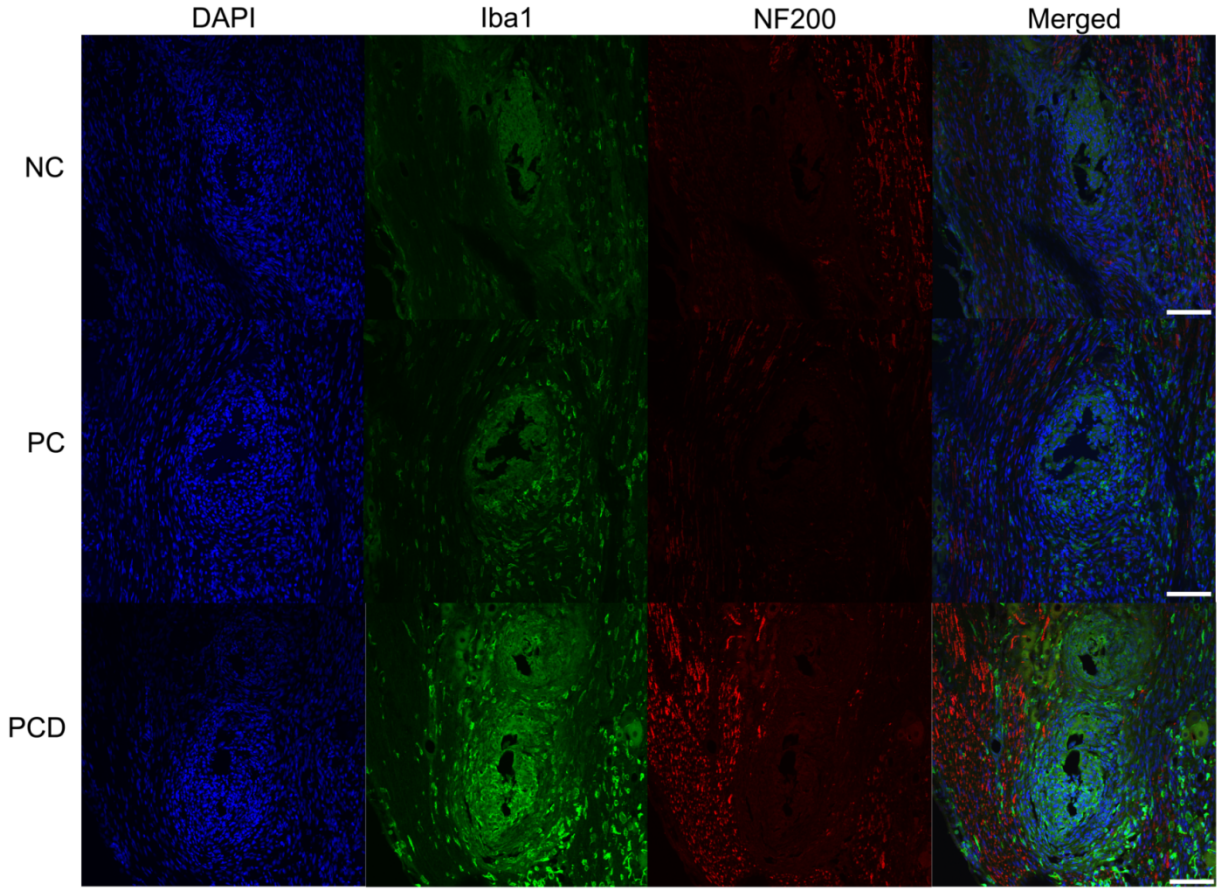

Figure 2-6. NF-200 and Iba-1 expression in the DRG after chronic stimulation. Immunofluorescence images of rat DRG stained for NF200 (red) and Iba1 (green). NF200 staining was lacking in the area immediately surrounding the implant site and differences

assessed by measuring the size of the area void of this staining. Iba1-positive cells were localized around the implant site and this increased immunoreactivity quantified and compared. Representative images from each of the coating conditions after stimulation are provided. Scale bars represent 100 μm.

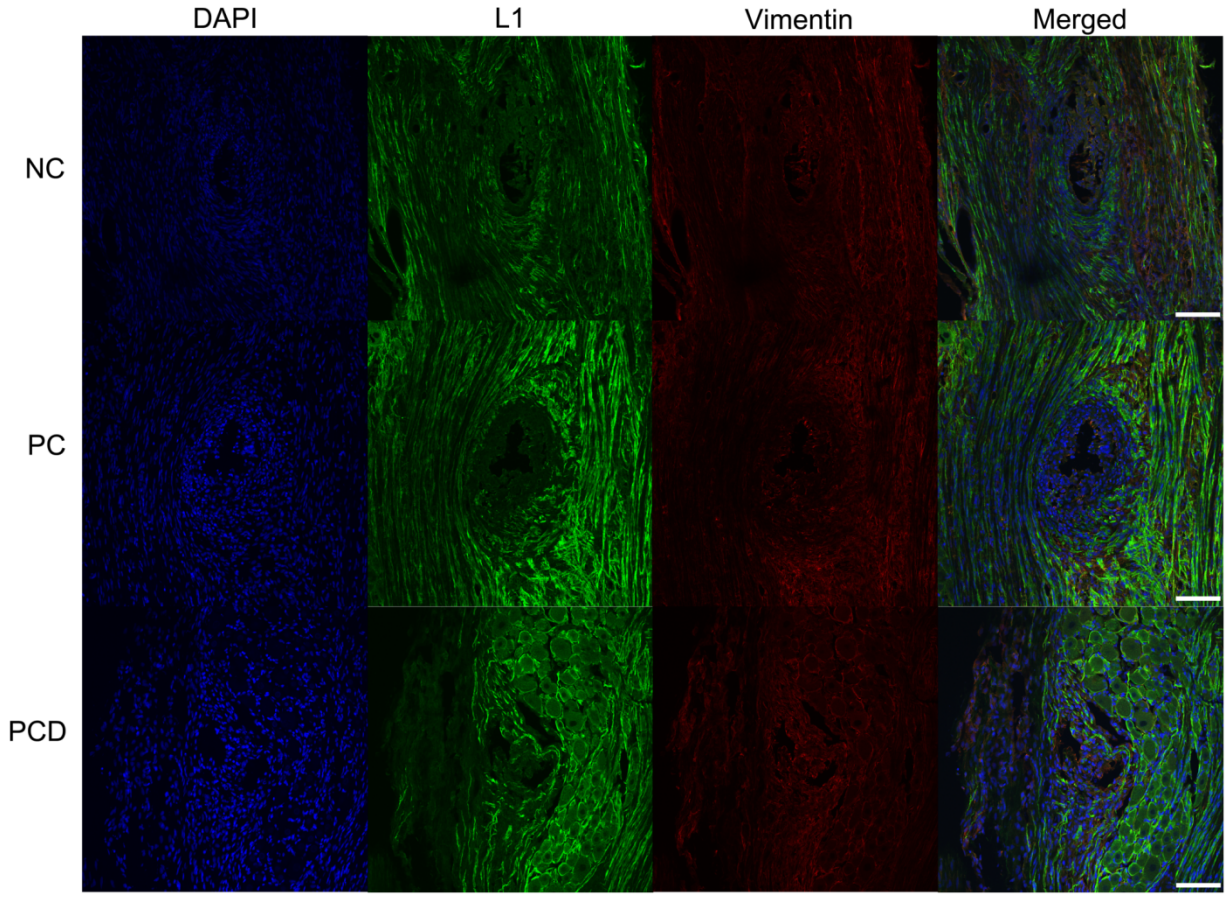

Figure 2-7. L1 and vimentin expression in the DRG after chronic stimulation. Immunofluorescence images of rat DRG stained for L1 (green) and vimentin (red) following implant of NC, PC and PCD neural probes. L1 staining was found around the implant site and associated with Schwann cells/peripheral myelin. Vimentin staining was relatively evenly distributed with some colocalization with L1. Representative images from each coating condition after stimulation. Scale bars represent 100 μm.

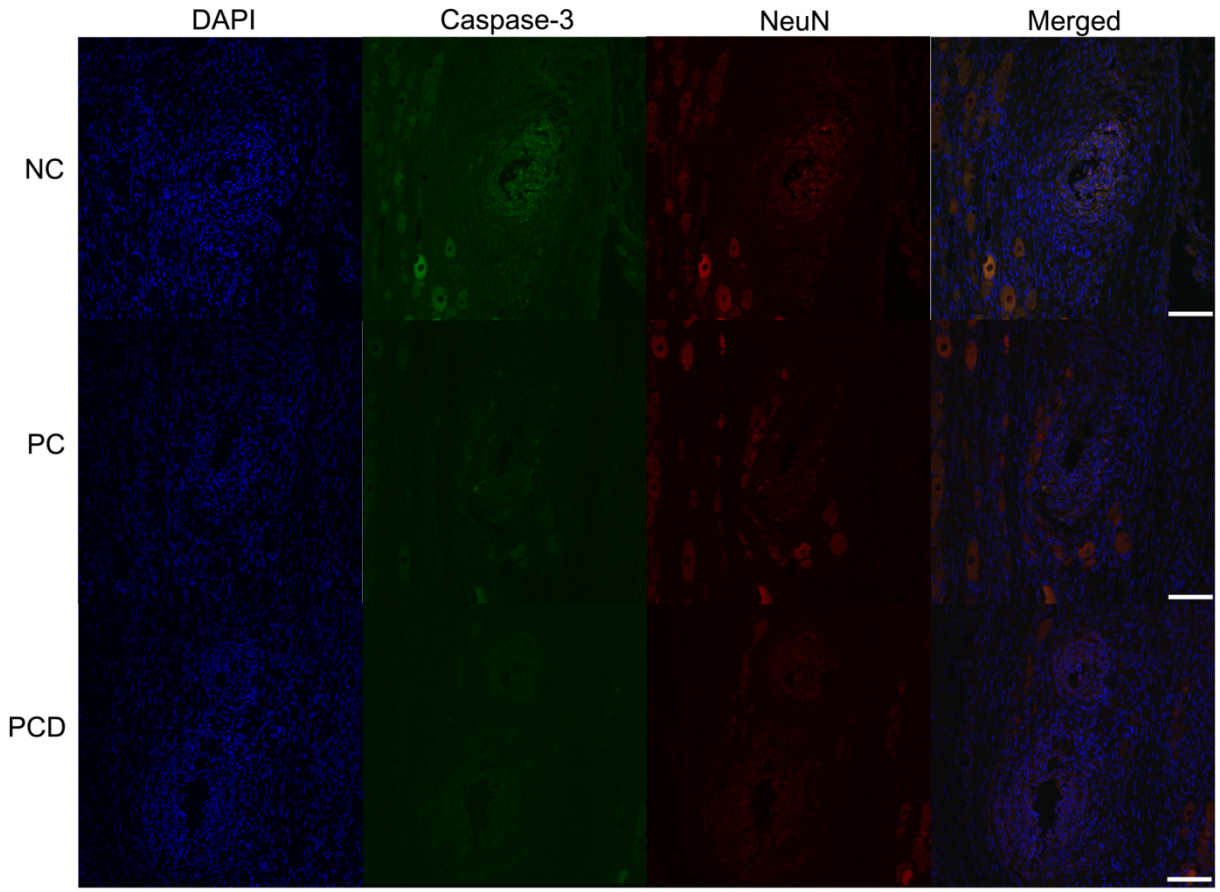

Figure 2-8. Colocalization of NeuN and activated caspase-3 in the DRG after chronic stimulation. Immunofluorescence images were used to determine the degree of co-localization between NeuN (red) and cleaved caspase-3 (green) and representative images provided. The number of NeuN/caspase-3 positive cells was quantified and reported as a percentage of the total number of NeuN positive cells. Representative images are provided from each of the three coating conditions. Scale bars represent 100 μm.

Plans: We plan to submit a manuscript based on this work in early September to the Journal of Neural Engineering.

Key Research Accomplishments in last year

Project 2. Establishment of Neural interface stability and optimization

Milestones	Progress
Histological evaluation of implant sites	Completed the tissue response evaluation for the untreated and L1 treated electrodes implanted acute and chronically in DRG and spinal cord.
Implant surgeries for tissue reaction to chronic stimulation study.	Applied PEDOT/CNT and PEDOT/CNT/Dexamethasone coatings for the stimulation electrodes. Completed the animal implantation and stimulation.
Histological evaluation of implant sites	All of the histological stains have been completed. Imaging has been completed. Manuscript in preparation.

Reportable Outcomes

Project 2. Establishment of Neural interface stability and optimization

1) Kolarcik, C.L., Bourbeau, D., Azemi, E., Rost, E., Zhang, L., Lagenaur, C.F., Weber, D.J. and Cui, X.T. (2012). *In vivo effects of L1 coating on inflammation and neuronal health at the electrode/tissue interface in rat dorsal root ganglion and spinal cord*. *A*cta Biomater http://dx.doi.org/10.1016/j.actbio.2012.06.034.
2) Christi L. Kolarcik, Erika Rost, Ingrid Albrecht, Xiliang Luo, Kasey Catt, Douglas J. Weber and X. Tracy Cui. Response of dorsal root ganglion tissue to chronic stimulating electrodes. Abstract submitted to the Federation of American Societies for Experimental Biology meeting in April of 2012; selected for presentation at a special session on Cell Injury sponsored by the American Society for Investigative Pathology
3) Christi L. Kolarcik[a], Dennis Bourbeau[b], Erdrin Azemi[a,c], Erika Rost[a], Ling Zhang[a], Carl F. Lagenaur[c,d], Douglas J. Weber[b] and X. Tracy Cui, In vivo effects of L1 coating on inflammation and neuronal health at the electrode/tissue interface in rat dorsal root ganglion and spinal cord, final stage of proof reading, to be submitted to Biomaterials
4) Luo, X., C. L. Weaver, D. D. Zhou, R. Greenberg, and X. T. Cui, Highly stable carbon nanotube doped poly(3,4-ethylenedioxythiophene) for chronic neural stimulation. Biomaterials, 2011. 32(24): p. 5551-5557.
5) Luo, X., C. Matranga, S. Tan, N. Alba, and X. T. Cui, Carbon nanotube nanoreservior for controlled release of anti-inflammatory dexamethasone. Biomaterials, 2011. 32(26): p. 6316-6323.
6) Stauffer, W. R., P. M. Lau, G. Q. Bi, and X. T. Cui, Rapid modulation of local neural activity by controlled drug release from polymer-coated recording microelectrodes. J Neural Eng, 2011. 8(4): p. 044001.
7) Collinger, J. L., B. E. Dicianno, D. J. Weber, X. T. Cui, W. Wang, D. M. Brienza, and M. L. Boninger, Integrating rehabilitation engineering technology with biologics. PM R, 2011. 3(6 Suppl 1): p. S148-157.
8) Cassandra L. Weaver, Xinyan Tracy Cui: Directing Neuronal Differentiation Via Neurochemical Release From Carbon Nanotube-doped Conducting Polymers, Society for Biomaterials meeting 2011, April, Orlando, FL
9) Xiliang Luo, Cassandra Lynn Weaver, David Daomin Zhou, Robert Greenberg, Xinyan Tracy Cui, Carbon Nanotube Doped Poly(3,4-Ethylenedioxythiophene) for Chronic Neural Stimulation, Society for Biomaterials meeting 2011, April, Orlando, FL

10) Xinyan Tracy Cui, Bioengineering Approach Targeting Neuronal Loss and Glial Scar Around Neural Probes, invited lecture in Engineering Neural Interface Session, Gordon Research Conference on Biomaterials & Tissue Engineering, Plymouth, NH, 2011
11) Xinyan Tracy Cui, Improving Neural Implant Biocompatibility via Biomimetic Surface Design, invited seminar at CMU ECE department, April 2011, Pittsburgh
12) Christi L. Kolarcik, Dennis Bourbeau, Erdrin Azemi, Erika Rost, Ling Zhang, Carl F. Lagenaur, Douglas J. Weber and X. Tracy Cui, In vivo effects of L1 coating on inflammation and neuronal health at the electrode/tissue interface in rat dorsal root ganglion and spinal cord, Biomedical Engineering Society Meeting, October 2011, Hartford, CT.

References

1. McCreery, D., V. Pikov, and P.R. Troyk, *Neuronal loss due to prolonged controlled-current stimulation with chronically implanted microelectrodes in the cat cerebral cortex.* J Neural Eng, 2010. **7**(3): p. 036005.

Project 3. Virtual reality environment for prosthetic training and testing

Objectives

The goal of this year was to focus primarily on human subject testing in both able-bodied individuals and those with disabilities due to limb amputation or spinal cord injury. The testing included:

1. MEG Testing: Using magnetoencephelography (MEG) neural/brain activities were recorded from ten subjects including healthy controls and individuals with amputation. In the first part of the experiment, these signals were recorded when subjects performed movements or observed movements performed by virtual arm and hand. In the second part of the experiment, by using the signals in the contra-lateral brain, subjects were able to control two synergies/movement primitives of a high dimensional virtual hand. For each of the subjects who participated in this study we also performed an MRI scan to help us in source localization of the MEG signals.

   Same ten subjects also participated in EMG testing discussed as follows.

2. EMG Testing: Using surface electromyographic (EMG) signals, muscle activities were recorded from ten subjects. By using these signals, subjects were able to control two or three synergies/movement primitives of a high dimensional virtual hand.

Chapter organization

This chapter is organized as follows. Section titled Software describes the custom software, Craniux that was developed in our laboratory for human-machine interface applications. Section titled Paradigms, explains in detail the experimental paradigms used to extract meaningful brain signals for scientific analysis as well as dexterous control of virtual hand. Section titled Results, presents the promising preliminary results that we have achieved. Both Paradigms and Results have two subsections for MEG and EMG testing.

Software

For all the experiments in MEG and EMG testing we have used our custom developed software Craniux was used. Craniux is an extensible software suite for Brain-Machine Interface research (BMI), developed using LabVIEW (National Instruments, Inc.), a high-level multi-platform graphical development environment. Craniux implements a core framework for BMI operation, including modular architecture, network communication between modules, data flow control, data visualization, data storage, graphical user interfaces and has the ease of efficiently communicating with rich virtual reality environments such as Unity 3d. The Craniux software package has been designed to be a highly modularized system, capable of operating across both a distributed network of computers and on a single computer. Fig.3-1 illustrates the core modules in the Craniux system architecture. There are three important modules 1. Acquisition: for acquiring neural or muscle control signals, 2. Signal Processing: for performing spectral estimations and decoding the intent behind the control signals and 3. Application: for using the decoded control signal in applications such as virtual hand control in this study.

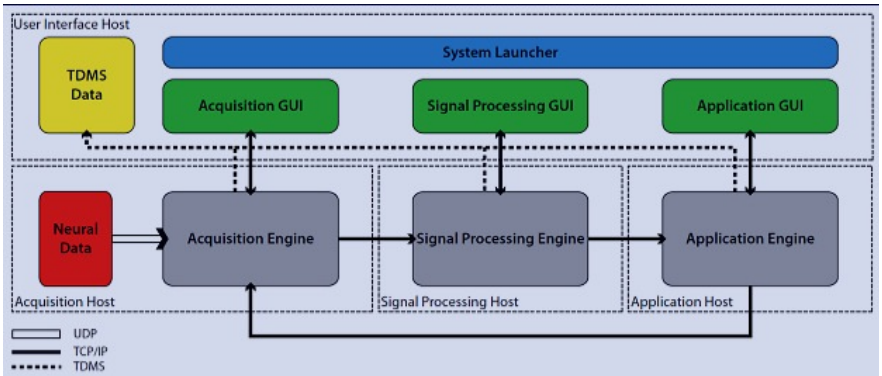

Fig. 3-1. Craniux System Architecture

This software has been used extensively in all the open-loop and as well as closed-loop real-time experiments conducted in this study.

Paradigms

MEG signals for hand and arm control

Using magnetoencephelography (MEG) neural/brain activities were recorded from ten subjects including healthy controls and individuals with amputation. MEG is an established neural recording methodology that offers high temporal resolution with sufficient spatial resolution. There were two parts to the experiment. In the first part of the experiment, these signals were recorded when subjects performed movements or observed movements performed by virtual arm and hand. These two tasks were termed as action execution and observation respectively. Studies done previously by us and others have shown that similar neural activities were observed during action execution and action observation. Thus the action observation task gives a close approximation to the neural signals action execution for amputees. In the second part of the experiment, by using the signals in the contra-lateral brain, subjects were able to control two synergies/movement primitives of a high dimensional virtual hand. For each of the subjects who participated in this study we also performed an MRI scan to help us in source localization of the MEG signals.

1. Neural signal modulation during action observation and action execution:

As discussed previously in this first part of the experiment, neural signals were recorded when subjects performed movements or observed movements performed by virtual arm and hand. These two tasks were termed as action execution and observation respectively. A brief description of these tasks follows.

Setup: The subject is seated in MEG machine as show in Fig.3-4 with their hands resting on the plank placed in front of them. The virtual hand is projected onto a projector placed in front of the subject. A total of 306 channels of MEG data including 204 gradiometers, and 102 magnetometers are recording the neural data during the session. To measure eye movement artifacts, electro-oculograms are recorded to take into account eye blinks and eye side glances. Four head position coils are placed on top of the head in a square design to monitor the head position.

Action Execution (AE):

In this task, the subjects were comfortably seated in MEG machine with their arms/hands resting on resting pad placed in front of them. They were wearing MRI-compatible 5DT data glove that can measure the joint angles of the hand. For all healthy controls, their dominant hand was used in performing the actual movements. Only unilateral amputees participated in this study. In their case, the healthy hand was used for performing actual movements.

Subjects were visually presented with pictures of 9 different hand postures corresponding to – 1. Thumb flexed 2. Index finger flexed 3. Middle finger flexed 4. Ring finger flexed 5. Pinky finger flexed 6. Whole hand flexed 7. Synergy 1 (Thumb and Index finger flexed) 8. Synergy 2 (Middle, Ring and Pinky fingers flexed) and 9. Wrist flexed. These 9 different postures were presented in a random order to the subjects. When prompted subjects were asked to perform this movement. During this movement the hand kinematics and neural signals were recorded for later analysis. Between the movements there was a 2s rest period where the subjects were resting with their hand relaxed.

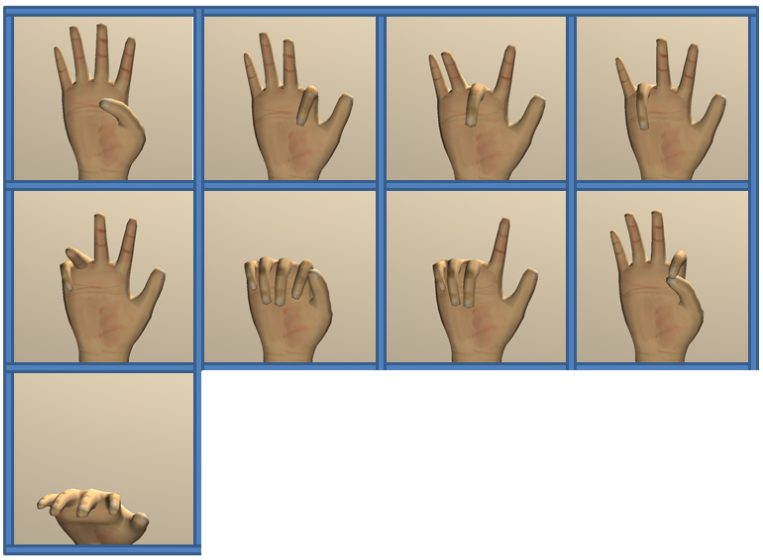

Figure 3-2. Subjects were visually presented with pictures of 9 different hand postures corresponding to 1. Thumb flexed 2. Index finger flexed 3. Middle finger flexed 4. Ring finger flexed 5. Pinky finger flexed 6. Whole hand flexed 7. Synergy 1 (Thumb and Index finger flexed) 8. Synergy 2 (Middle, Ring and Pinky fingers flexed) and 9. Wrist flexed.

Action Observation (AO):

In this task, the subjects were prompted by the movements of virtual hand that performed the entire movement starting from open hand to end at the above 9 postures. During these 9 different postural movements the subjects were observing the virtual hand making the movements. Please note that, in contrast to the picture stimuli shown in the Action Execution task, in this task, actual movements of virtual hand were presented as stimulus.

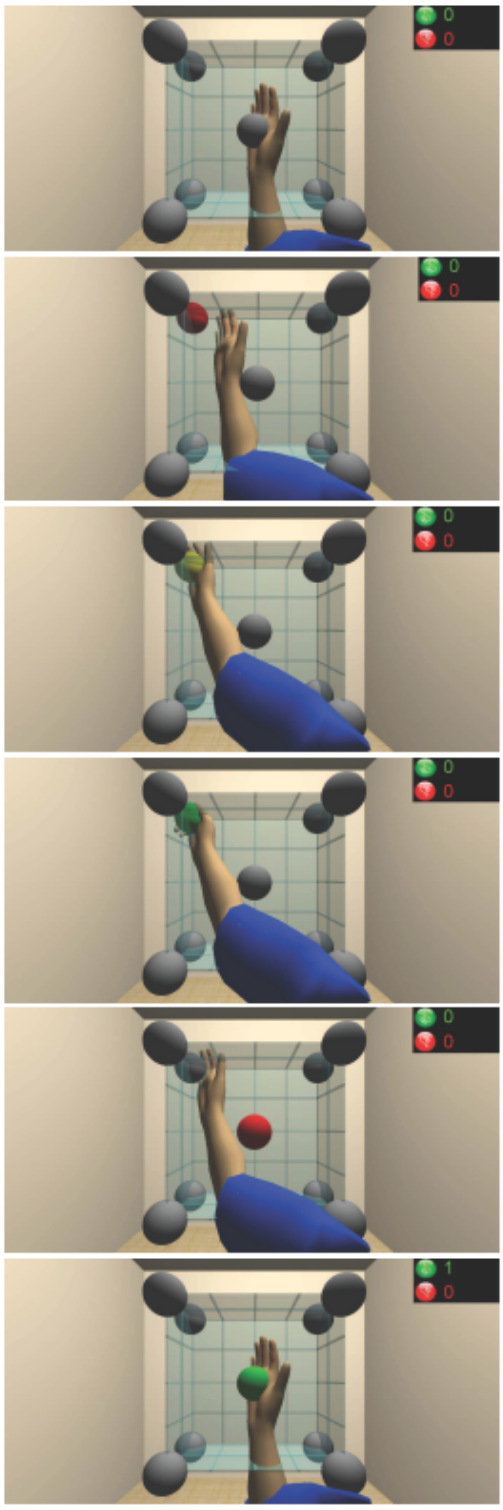

Figure 3-3. A virtual reality environment setup to emulate a virtual arm reaching and grasping the targets placed on corners of the glass cube. Gradual progression of movement phases, of which reach, grasp, release, return were displayed to the subject.

Observing Virtual Arm Reaching:

In this task, the virtual arm gradually moved from the center target to one of the peripheral targets. This was achieved in the following way. A gradual progression of movement phases: 1. Rest/idle 2. Reach for target 3. Reach (target turns yellow from red on success) 4. Grasp (target turns green from yellow on success) 5. Release (target turns gray from green and center target turns red) 6. Return (center target turns green on success) were shown in Figure 3-3. The subject was instructed to observe the moving arm and while grasping to perform grasping their hand. This paradigm was designed to see if we can decode directional modulation in the neural signals while subjects were observing the arm movements. Performing the grasp, during grasp phase was embedded to keep the subjects active during the session.

2. Real time control of synergies of a virtual hand using MEG signals:

Introduction: In this task, the subjects were given full brain control of the two synergies shown in Fig. 3-2. These are called synergies as the movement is synergistic movement across multiple fingers. The idea behind controlling synergies is that, the control of two synergies instead of two joints can lead to multidimensional control of useful functional degrees of freedom of human or robotic hand that can benefit the end users in their activities of daily living.

Setup: The subject is seated in MEG machine as show in Fig.3-4 with their hands resting on the plank placed in front of them. The virtual hand is projected onto a projector placed in front of the subject. A total of 306 channels of MEG data including 204 gradiometers, and 102 magnetometers are recording the neural data during the session. To measure eye movement artifacts, electro-oculograms are recording to take into account eye blinks and eye side glances. Four head position coils are placed on top of the head in a square design to monitor the head position.

Fig.3-4 shows schematic of real time MEG. From the signal processing engine of MEG machine, data is streamed in 50ms chunks to a buffer (FieldTrip Buffer) and a second system extracts data via TCP/IP to perform data processing with the Craniux BMI software. During real time control visual feedback is updated based on the decoded neural signals.

Task Training: Two virtual hands were projected onto the screen. The left virtual hand corresponded to target hand posture. The right virtual hand corresponds to the controllable hand. During training the right virtual hand is completely controlled by computer to reach to the target posture shown by the left hand. The task begins with training, where the subjects were asked (i) to squeeze their hand when the virtual hand performed Synergy 1 (ii) to flex their ankle when the virtual hand performed Synergy 2 (iii) to squeeze their hand and flex their ankle simultaneously when the virtual hand performed whole hand flexion because this is achieved by combination of the two synergies and (iv) to relax when the virtual hand is open palm with no movement. After training for 10 repetitions of each of the above conditions, the collected data is used in training an optimal linear estimator based decoder.

Signal Processing: Using decreases in sensorimotor rhythms (SMR) over contralateral hand area during attempted hand/ankle movement (i.e. 8-28Hz), the neural data that is being modulated is used for

controlling the two synergies. SMR modulations during hand flexion and ankle flexion were used to directly command the movement of a virtual hand.

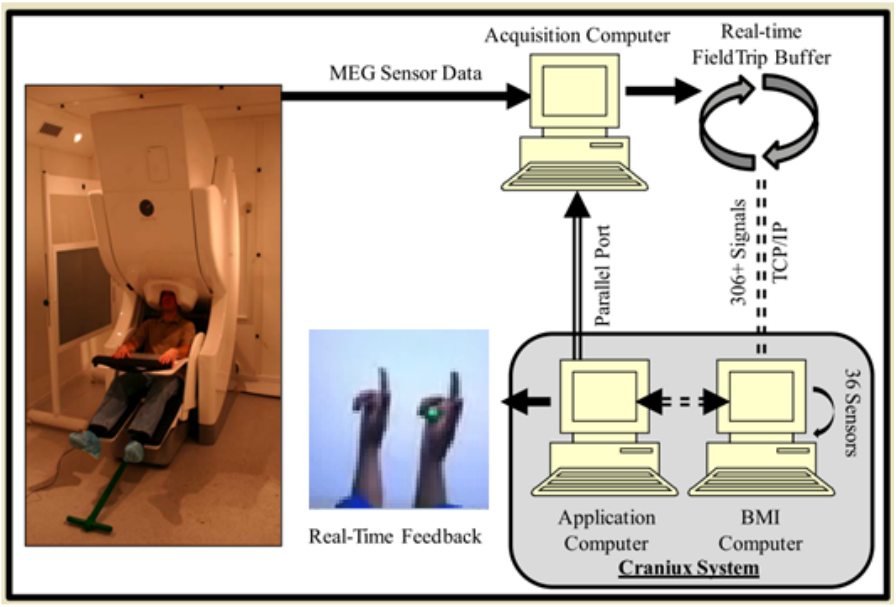

Figure 3-4. Real-Time MEG System Schematic with the Elekta Neuromag. Data is streamed in 50ms chunks to a buffer (FieldTrip Buffer) and a second system extracts data via TCP/IP to perform data processing with the Craniux BMI software described below. Feedback is updated based on the decoded neural signals.

Spectral powers of the neural signals were calculated with 6Hz resolution centered at 9, 15, 21, 27 Hz. 300 ms window sliding at 50 ms update rate was used. The neural signals recorded from 36 gradiometers, which resulted in up to 144 neural features were used for decoding. An optimal linear estimator was used to linearly map neural features to commands. Only features correlated with task with $R^2 > 0.01$ were used in the decoder.

Testing: During testing, the subject is given full control of the controllable (right) hand. The target posture, similar to training, is indicated by the left hand. The output of the decoder controlled the joint angular velocity of the fingers involved in either synergy 1 or Synergy 2. By modulating either hand flexion or ankle flexion the subjects controlled the virtual hand.

Data Summary: Following is a table of summary of the MEG and MRI data collected for all 11 subjects enrolled (1 withdrawn).

Session Subject	Session1 MEG Signals during AO/AE	Session2 MEG Signals during AO/AE	Session2 Real time control using MEG signals	MRI Scan
VRA	✓	✓	✓	✓
VRB	✓	✓	✓	✓
VRC	✓	✓	✓	✓
VRD	✓	✓	✓	✓
VRE	×	×	×	✓
VRF	✓	✓	✓	✓
VRG	✓	✓	✓	✓
VRH	✓	✓	✓	✓
VRI	✓	✓	✓	✓
VRJ	✓	✓	✓	✓
VRK	✓	✓	✓	✓

EMG signals for Dexterous Hand Movement Control

Prosthetic hands give hope for amputees to recapture their ability to perform complicated physical movements of the lost human hands. Electromyography (EMG) is a suitable approach for human-machine interface in the prosthetic hands control as it is noninvasive and offers reliable control. The first artificial hand controlled by EMG was developed by A. E. Kobrinski in 1961. Since then several versions of EMG based prosthetic controllers are available. Using EMG to control synergies, we discussed in the previous section, has never been implemented. As explained earlier, the benefits of synergy based control, the user can control useful multiple dimensions for activities of daily living.

In this study by using surface EMG signals ten subjects including healthy subjects and amputees have demonstrated the control of two and three synergies. Each of the control paradigms is explained here.

1. Two synergies:

Setup: The subjects are seated comfortably in a chair and are seated in front a computer monitor that displays the target virtual hand (left) and the virtual hand they are controlling (right). Two electrodes are placed on forearm flexor muscle and biceps respectively. A third electrode for reference is placed on ankle bone. These electrodes are connected by insulated wires that lead to the amplifier placed on the right side of the table. The success or failure of the grasp is indicated graphically on the screen, the score is updated and also via speakers that carried different sounds for success and failure. The acquisition computer and the amplifier are powered by an isolation transformer to be free from ambient noise.

Figure 3-5. Real-Time EMG control setup showing the display monitor, the amplifier (right), placed in front of the subject seated comfortably in a chair. The subject achieved the target posture and was indicated by ball in the hand turning green. Subject blurred for privacy protection.

Training: Very similar to the two synergy control explained under MEG testing, the task here begins with training. Two virtual hands were projected onto the screen. The left virtual hand corresponded to target hand posture. The right virtual hand corresponds to the controllable hand. During training the right virtual hand is completely controlled by computer to reach to the target posture shown by the left hand. The subjects were asked (i) to contract their forearm flexors when the virtual hand performed Synergy 1 (ii) to contract their biceps when the virtual hand performed Synergy 2 (iii) to contract both muscles simultaneously when the virtual hand performing whole hand flexion because this is achieved by combination of the two synergies and (iv) to relax when the virtual hand is open palm with no movement. After training for 10 repetitions of each of the above conditions (40 repetitions is one block), the collected data is used in training an optimal linear estimator based decoder.

Signal Processing: Signals from the EMG electrodes were recorded with a g.USBamp Biosignal Amplifier (g.tec Medical Engineering), and sampled at 1200 Hz. The signals were filtered and processed using the Craniux. Spectral estimation was performed using the Burg AR method over the 10 to 200 Hz range (25th order, 10 Hz band width). The frequency band was chosen as is appropriate for EMG. Estimates were calculated every 33 ms using a sliding window of 300 ms of raw data. AR data were log-transformed, then normalized to pseudo Z-scores relative to a baseline/rest condition. These spectral estimates for each frequency band were used as the features for online control. The features (2 electrodes x 20 bands = 40 in total) were used for training, decoding, and control.

The neural decoder part of the Craniux system employed the optimal linear estimation (OLE) algorithm to determine a mapping between these neural features and cursor movement. This mapping took the

form of a matrix of weights (W) to be applied to the neural features (f) for decoding, i.e. the two dimensions of cursor movement velocity ($\hat{v}$) were each a weighted sum of neural feature input, based on Equation 1. The decoding weights were calculated using the optimal linear estimator (OLE) algorithm based on Equation 2:

$$\hat{v} = fW \tag{1}$$

$$W = F^{+}V \tag{2}$$

where V and F are matrices representing the desired cursor movement direction and associated neural features, respectively. The desired cursor movement direction is the instantaneous unit vector pointing from the cursor to the target, averaged over a trial. The superscript "+" denotes pseudo-inverse of a matrix. Initial values for V and F were acquired from one block of trials where the monkey followed an automatically guided cursor with his hand. Each subsequent update of the decoder used all trials from a single block.

Testing: During testing, the subject is given full control of the controllable (right) hand. The target posture, similar to training, is indicated by the left virtual hand. The output of the decoder controlled the joint angular velocity of the fingers involved in either Synergy 1 or Synergy 2. By modulating either forearm flexor muscle contraction or biceps contraction the subjects controlled the virtual hand. A second testing set was introduced that contained partial postures of the four conditions listed during training. The subjects had to control their muscle contraction to stop at half the flexion instead of completing the flexion. The subjects were able to easily adapt their muscle contractions to achieve this task.

2. Three synergies:

Setup: The setup is very similar to two synergies task. Except, in this task, three (instead of 2 in previous task) electrodes are placed on forearm flexor muscle, biceps and trapezius muscles respectively. A fourth electrode for reference is placed on ankle bone.

Training: Similar training is adapted here also as compared to previous task. The subjects were asked (i) to contract their forearm flexors when the virtual hand performed Synergy 1 (ii) to contract their biceps when the virtual hand performed Synergy 2 (iii) to contract their trapezius when the virtual hand performed Synergy 3 (iv) to contract all three muscles simultaneously when the virtual hand performing whole hand flexion because this is achieved by combination of the three synergies and (v) to relax when the virtual hand is open palm with no movement. After training for 10 repetitions of each of the above conditions (40 repetitions is one block), the collected data is used in training an optimal linear estimator based decoder. The three synergies in this task are show in Fig.3-6 below.

Signal Processing: Same as in the previous section, the only difference being the decoder gives out three output control signals to control three synergies of this task.

Figure 3-6. Synergies used in three synergy control. Note that these are non-overlapping movements.

Testing: By modulating either forearm flexor muscle contraction or biceps contraction or trapezius contraction the subjects controlled the virtual hand. A second testing set was introduced that contained combinations of the three synergies used in training. The subjects had to adapt to the combinations of different muscle contractions to achieve the target postures. The subjects were able to easily adapt their muscle contractions to achieve this task.

Data Summary

Following is a table of summary of the EMG data collected for all 11 subjects enrolled (1 withdrawn).

Session **Subject**	**Session 1** Two synergy Training and Testing	**Session 2** Two synergy Testing	**Session 3** Two synergy Testing	**Session 4** Three synergy Training and Testing	**Session 5** Three Synergy Testing	**Session 6** Three Synergy Testing
VRA	✓	✓	✓	✓	✓	✓
VRB	✓	✓	✓	✓	✓	✓
VRC	✓	✓	✓	✓	✓	✓
VRD	✓	✓	✓	✓	✓	✓
VRE	×	×	×	×	×	×
VRF	✓	✓	✓	✓	✓	✓
VRG	✓	✓	✓	✓	✓	✓
VRH	✓	✓	✓	✓	✓	✓
VRI	✓	✓	✓	✓	✓	✓
VRJ	✓	✓	✓	✓	✓	✓
VRK	✓	✓	✓	✓	✓	✓

Results

MEG signals for during hand and arm control

Action observation and Action execution:

Following figure shows the brain activity for one of the subjects, for action observation: where the subjects were observing virtual hand grasp and for action execution: where the subjects performed virtual hand grasp. Both images were constructed on the subject specific anatomical brain model that was constructed using his/her structural MR scan. The results are Dynamical Statistical Parameter Mapping (dSPM) values (i.e. statistical values), using minimum norm estimate (MNE) on subject specific brain using Boundary Element Method (BEM). It is observed that during both observation and execution the occipital cortex is active due to the visual stimulus, sensorimotor activity in the motor cortex due to either performing the action or observing the action. Although motor cortical activity is present during both action observation and action execution, it appears to be predominant during action execution. The data are averages of 75 trials per condition and are initially cleaned with tSSS (Spatio-temporal Signal Space Separation).

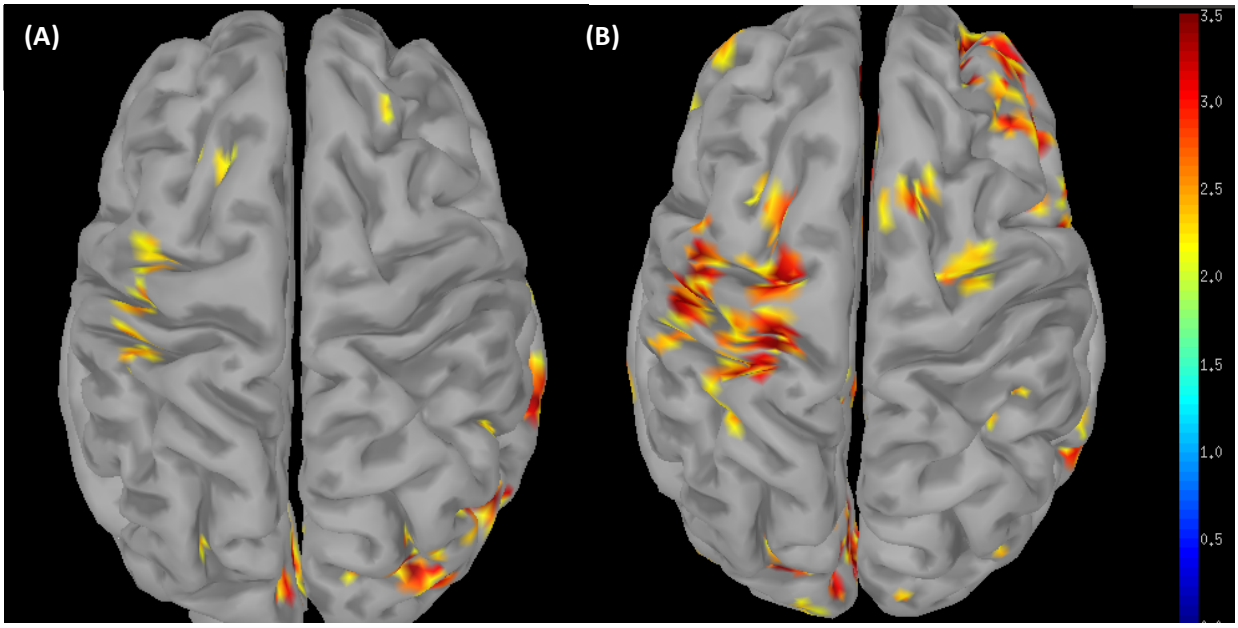

Figure 3-7. Neural source activity during action observation (A) and action execution (B) averaged across 75 trials for one subject shown above. Activity is plotted as dSPM values (noise-normalized MNE) near 720 ms after stimulus onset (using Brainstorm-Toolbox). dSPM color scale and parameters are the same across all action observation and execution. Motor activity is seen during both tasks in motor areas (less intense during action observation).

Two synergy control:

Following shows the power spectrum during two synergy real-time control from one sensorimotor gradiometer during two cases - (A) using imagination as control strategy and (B) using action execution as control strategy. First and second synergies are controlled in A and B respectively. The dotted line is the start of the trial. Spectrograms shown in the figure reflect percentage change from baseline. A one minute baseline data is collected at the beginning of the real-time session, where the subject is instructed to remain relaxed.

It is observed that the sensorimotor rhythms become more 'desynchronized' when one of the synergies is controlled. In both figures the red and green refer to the joint positions of the finger joints involved in that synergies one and two respectively. These are obtained by integrating the joint angular velocities generated by the decoder output control signals. It is observed that in both cases, when the subject is achieving control, the subject dissociates the two control signals, making them more independent, thus demonstrating 2 degree of freedom control.

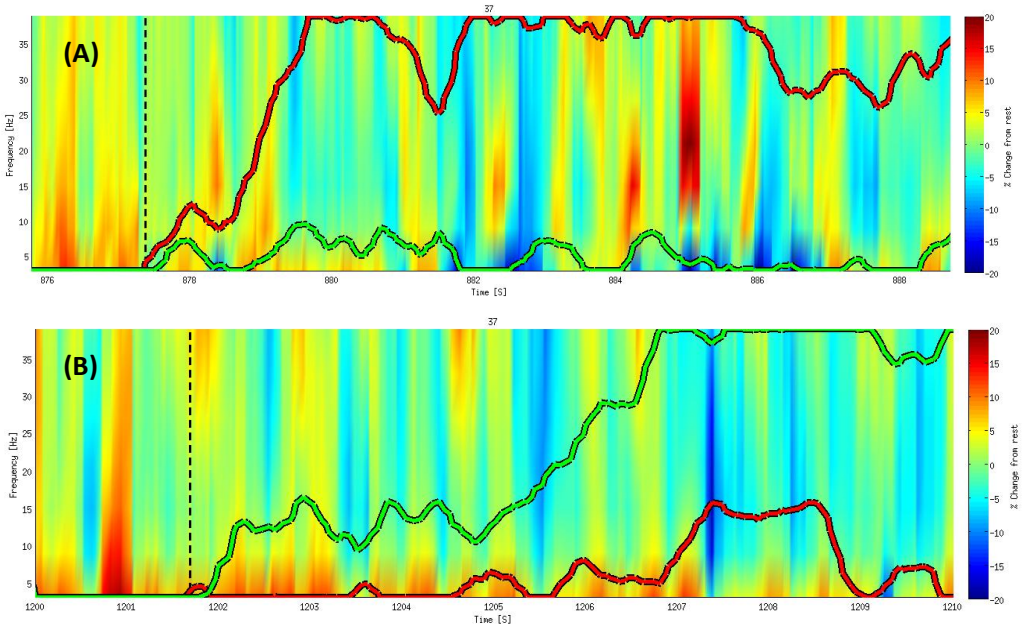

Figure 3-8. Two synergy real-time control using (A) action imagination (B) action execution. The power spectrum during real-time synergy control from one sensorimotor gradiometer during two cases A and B. First and second synergies are controlled in A and B respectively. The dotted line is the start of the trial. Spectrograms shown in the figure reflect percentage change from baseline.

EMG signals for Dexterous Hand Movement Control

Two synergies:

During this control, two synergies shown on the left are controlled by two control signals that are the outputs from the decoder. The output of the decoder is a velocity control signal, that control the joint angular velocities of the finger joints involved in a particular synergy. The top row indicates the target postures that needed to be achieved. This subject learned to control the two synergies to combine them uniquely to achieve the target postures. For example, Target code 3 refers to whole hand flexion that involves combination of both the synergies. Hence you see activation in both control signals controlling the synergies. Target code 4 corresponds to activation of only first synergy and hence the same is reflected in the control signal. The blank target posture corresponds to open palm or relaxed posture where the subject is relaxed and is not using either of the synergies. Although the subjects achieved successful control of synergies, nevertheless, the subjects could not completely avoid the interference of muscle activities. For example, during Target code 1 the subject only needs to activate synergy 2, but we observe that both control signals are active. Also note that the time taken by the subject to achieve this posture also is longer. During the later phase, the subject suppressed the control signal 1, and held control signal 2 high that eventually led to success. All the subjects were trained only for 5 minutes before they achieved this type of control. Given sufficient training, we believe that subjects can learn to elicit individuated controls signals.

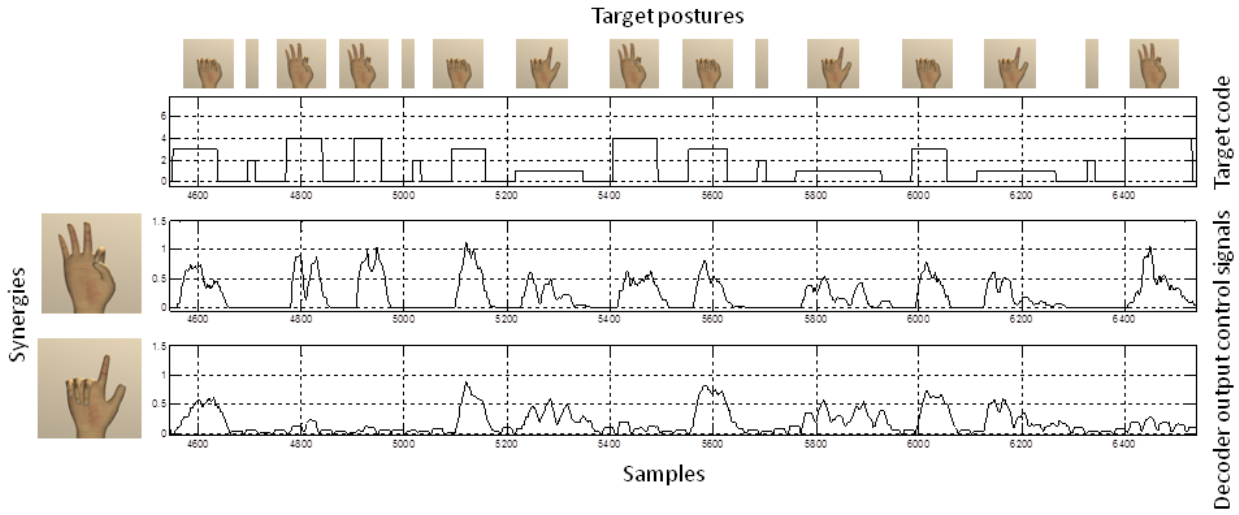

Figure 3-9. Two synergy control: Two synergies shown on the left are controlled by two control signals that are the outputs from the decoder. The top row indicates the target postures that needed to be achieved. This subject learned to control the two synergies to combine them uniquely to achieve the target postures. The blank target posture corresponds to open palm or relaxed posture where the subject is relaxed and is not using either of the synergies.

Three synergies:

During this control, three synergies shown on the left are controlled by three control signals that are the outputs from the decoder. Similar to two synergy control the output of the decoder is a velocity control signal, that control the joint angular velocities of the finger joints involved in a particular synergy. The top row indicates the target postures that needed to be achieved. This subject learned to control the three synergies to combine them uniquely to achieve the target postures. For example, Target code 4 refers to whole hand flexion that involves combination of three synergies. Hence you see activation in three control signals controlling the synergies. Target code 5 corresponds to activation of first and second synergies and hence the same is reflected in the control signals. Target code 5 corresponds to activation of first and second synergies and hence the same is reflected in the control signals. Target code 7 corresponds to activation of first and third synergies and hence the same is reflected in the control signals. The blank target posture corresponds to open palm or relaxed posture where the subject is relaxed and is not using either of the synergies. Although the subjects achieved successful control of synergies, nevertheless, the subjects could not completely avoid the interference of muscle activities. For example, during Target code 6 the subject needs to activate synergies 2 and 3, but we observe that all control signals are active. Also note that the time taken by the subject to achieve this posture also is longer. During the later phase, the subject suppressed the control signal 1, and held control signals 2 and 3 high that eventually led to success. All the subjects were trained only for 5 minutes before they achieved this type of control. Given sufficient training, we believe that subjects can learn to elicit individuated controls signals.

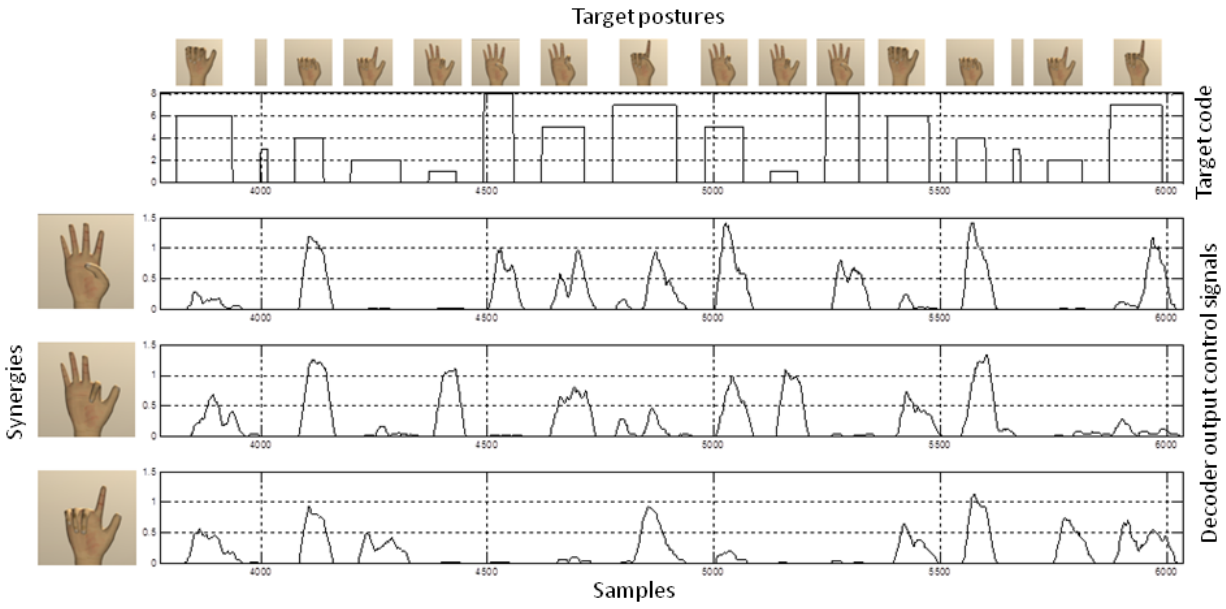

Figure 3-10. Three synergy control: Three synergies shown on the left are controlled by three control signals that are the outputs from the decoder. The top row indicates the target postures that needed to be achieved. This subject learned to control the three synergies to combine them uniquely to achieve the target postures. The blank target posture corresponds to open palm or relaxed posture where the subject is relaxed and is not using any of the synergies.

Publications:

Wang W, Degenhart AD, Collinger JL, Vinjamuri R, Sudre GP, Adelson PD, Holder DL, Leuthardt E, Moran DW, Boninger ML, Schwartz AB, Crammond DJ, Tyler-Kabara EC, Weber DJ (2009) Human motor cortical activity recorded with micro-ECoG electrodes during individual finger movements. In: IEEE EMBC. Minneapolis, MN, 2009.

Vinjamuri R, Degenhart AD, Collinger JL, Sudre GP, Adelson PD, Holder DL, Boninger ML, Schwartz AB, Crammond DJ, Tyler-Kabara EC, Wang W (2009) A fuzzy logic model for hand posture control using human cortical activity recorded by micro-ECoG. In: IEEE EMBC. Minneapolis, MN.

Vinjamuri R, Sun M, Weber D, Wang W, Crammond D, Mao Z-H (2009) Quantizing and characterizing the variance of hand postures in a novel transformation task. In: IEEE EMBC. Minneapolis, MN.

Wang W, Collinger JL, Perez MA, Tyler-Kabara EC, Cohen LG, Birbaumer N, Brose SW, Schwartz AB, Boninger ML, Weber DJ (2010) Neural interface technology for rehabilitation: exploiting and promoting neuroplasticity. Phys Med Rehabil Clin N Am 21:157-178.

Wang W, Sudre GP, Kass RE, Collinger JL, Degenhart AD, Bagic AI, Weber DJ (2010) Decoding and cortical source localization for intended movement direction with MEG. Journal of Neurophysiology 104: 2451-2461.

Guo C, Li X, Taulu S, Wang W, Weber DJ (2010) Real-time robust signal space separation for magnetoencephalography. IEEE Trans Biomed Eng 57:1856-1866.

Sudre G, Xu Y, Kass R, Weber DJ, Wang W (2010) Cluster-Based Algorithm for ROI Analysis and Cognitive State Decoding Using Single-Trial Source MEG Data. In: 17th International Conference on Biomagnetism Advances in Biomagnetism – Biomag2010 (Supek S, Sušac A, eds), pp 187-190: Springer Berlin Heidelberg.

Sudre G, Wang W, Song T, Kajola M, Vinjamuri R, Collinger J, Degenhart A, Bagic A, Weber DJ (2010) rtMEG: A Real-Time Software Toolbox for Brain-Machine Interfaces Using Magnetoencephelography. In: 17th International Conference on Biomagnetism Advances in Biomagnetism – Biomag2010 (Supek S, Sušac A, eds), pp 362-365: Springer Berlin Heidelberg.

Kelly JW, Siewiorek DP, Smailagic A, Collinger JL, Weber DJ, Wang W (2011) Fully automated reduction of ocular artifacts in high-dimensional neural data. IEEE Trans Biomed Eng 58:598-606.

Zhang J, Sudre G, Li X, Wang W, Weber D, Bagic A (2011) Group independent linear discriminant analysis for magnetoencephalography-based brain computer interfaces. IEEE Trans Neural Syst Rehab Engr.

Degenhart AD, Kelly JW, Ashmore RC, Collinger JL, Tyler-Kabara EC, Weber DJ, Wang W (2011) Craniux: a LabVIEW-based modular software framework for brain-machine interface research. Computational intelligence and neuroscience 2011:363565.

Sudre GP, Parkkonen L, Bock E, Sylvain B, Wang W, Weber, DJ (2011) rtMEG: a real-time software interface for magnetoencephalography. Comput Intell Neurosci.

Collinger JL, Dicianno BE, Weber DJ, Cui XT, Wang W, Brienza DM, Boninger ML (2011) Integrating rehabilitation engineering technology with biologics. PM & R : the journal of injury, function, and rehabilitation 3:S148-157.

Vinjamuri R, Weber DJ, Mao ZH, Collinger JL, Degenhart AD, Kelly JW, Boninger ML, Tyler-Kabara EC, Wang W (2011) Toward synergy-based brain-machine interfaces. IEEE transactions on information technology in biomedicine : a publication of the IEEE Engineering in Medicine and Biology Society 15:726-736.

Xu Y, Sudre GP, Wang W, Weber DJ, Kass RE (2011) Characterizing global statistical significance of spatiotemporal hot spots in magnetoencephalography/ electroencephalography source space via excursion algorithms. Statistics in medicine 30:2854-2866.

Wodlinger B, Degenhart AD, Collinger JL, Tyler-Kabara EC, Wang W (2011) The impact of electrode characteristics on electrocorticography (ECoG). Conf Proc IEEE Eng Med Biol Soc 2011:3083-3086.

Foldes ST, Vinjamuri RK, Wang W, Weber DJ, Collinger JL (2011) Stability of MEG for real-time neurofeedback. Conf Proc IEEE Eng Med Biol Soc 2011:5778-5781.

Degenhart AD, Collinger JL, Vinjamuri R, Kelly JW, Tyler-Kabara EC, Wang W (2011) Classification of hand posture from electrocorticographic signals recorded during varying force conditions. Conf Proc IEEE Eng Med Biol Soc 2011:5782-5785.

Kelly JW, Collinger JL, Degenhart AD, Siewiorek DP, Smailagic A, Wang W (2011) Frequency tracking and variable bandwidth for line noise filtering without a reference. Conf Proc IEEE Eng Med Biol Soc 2011:7908-7911.

Wang W, Degenhart AD, Sudre GP, Pomerleau DA, Tyler-Kabara EC (2011) Decoding semantic information from human electrocorticographic (ECoG) signals. Conf Proc IEEE Eng Med Biol Soc 2011:6294-6298.

Ashmore RC, Endler BM, Smalianchuk I, Degenhart AD, Hatsopoulos NG, Tyler-Kabara EC, Batista AP, and Wang W (Accepted). Stable Online Control of an Electrocorticographic Brain-Computer Interface using a Static Decoder. In: IEEE EMBC. San Diego, CA, 2012: 2012.

Kelly JW, Degenhart AD, Siewiorek DP, Smailagic A, and Wang W (Accepted). Sparse Linear Regression with Elastic Net Regularization for Decoding in Brain-Computer Interfaces. In: IEEE EMBC. San Diego, CA, 2012: 2012.

Wang W, Collinger JL, Degenhart AD, Tyler-Kabara EC, Schwartz AB, Moran DW, Weber DJ, Wodlinger B, Vinjamuri RK, Ashmore RC, Kelly JW, Boninger ML (In preparation) An Electrocorticography-Based Brain-Computer Interface in an Individual with Tetraplegia. To be submitted to PLoS ONE.

Wodlinger B, Bagic AI, Tyler-Kabara EC, and Wang W (In review). The Effects of Electrode Size and Spacing on Cortical Surface Recordings. Clinical Neurophysiology.

Zhang J, Li X, Foldes ST, Wang W, Collinger JL, Weber DJ, Bagic AI (In review) Decoding MEG from User-Specified Cortical Regions. IEEE Transactions on Neural Systems and Rehabilitation Engineering.

Helou LB, Wang W, Ashmore RC, Rosen CA, and Abbott KV (In review). Intrinsic Laryngeal Muscle Activity in Response to Autonomic Nervous System Activation. Laryngology.

Collinger JL, Wang W, Vinjamuri R, Degenhart AD, Sudre GP, Boninger ML, Tyler-Kabara EC, Weber DJ (In preparation) Mirror neuron-like response of electrocorticographic recordings during overt and observed hand movement.

R. Vinjamuri, A. D. Degenhart, R. C. Ashmore, J. Collinger, M. Boninger, W. Wang. A Virtual Reality Environment for Brain-Machine Interface Training. To be submitted to IEEE Transactions on Visualization and Computer Graphics.

Stephen Foldes, Wei Wang, Jennifer Collinger, Xin Li, Jinyin Zhang, Gustavo Sudre, Anto Bagić and Douglas J. Weber (2011). Accessing and Processing MEG Signals in Real-Time: Emerging Applications and Enabling Technologies, Magnetoencephalography, Elizabeth W. Pang (Ed.), ISBN: 978-953-307-255-5, InTech.

Project 4. Prosthetic hardware testing

Objectives

Little objective or validated information exists about the quality and functional reliability of prostheses. The primary objective for the FY06 funding period is to develop and assemble a testbed for life-cycle testing of a variety of prosthetic feet. In months 1-6, we will design the testing apparatus and acquire and assemble the hardware and software for testing. We will also complete pilot testing with a small number of prosthetic limbs to validate the system.

In FY07, we will use the testbed to perform life-cycle testing of a variety of prosthetic feet. In months 1-6, we will acquire representative samples of the most popular foot designs and create fixturing for attaching the feet to the testbed. In months 3-12, we will perform the life-cycle testing and analyze the data.

Results

Acquire prosthetic feet and completed pilot testing: Prosthetic feet from three different manufacturers was ordered. The feet being tested are as follows: three Freedom 1000 Sierras, three Ossur Reflex VSPs, and three Ohio Willow Wood Pathfinders (Table 1). Technical issues with the machine were resolved and pilot testing with a Freedom 1000 Sierra was completed. Pilot testing was done on actual specimens; starting with a Freedom 1000 Sierra at P3 loading level. This first test was completed successfully. Other feet will be tested at the P5 loading level. During the testing, position and force data was collected for each channel (heel and forefoot). This data will allow us to compare feet on the basis of stiffness and creep, along with pass and fail. A data analysis program was developed to calculate these parameters.

Procurement: All prosthetic feet from the three different manufacturers were received including Freedom FS Sierras, Ossur VSPs, and Ohio Willow Wood Pathfinder II. Teflon sheets and Teflon tape were also purchased. Teflon was used on the bottom of the loading surface of the plates on both actuators so that load application at foot was frictionless.

Testing with P5 loading level: During the static proof tests, a maximum force of 2240 N is applied in a downward direction for 30 seconds on the heel and forefoot consecutively. During the ultimate strength tests, force is applied separately on the heel and forefoot, increasing gradually from 3360N to 4480 N at the rate of 175N/ 20 seconds. During the fatigue tests, load is applied on both the heel and forefoot alternatively for 2,000,000 cycles at a frequency of 1 Hz followed by a final static proof test at the P5 loading level. Each foot is examined before and after every test and often during the fatigue test.

Results: ISO 10328 testing at the P5 loading level has been completed on all nine feet without any failures. One Pathfinder II failed under suspicious circumstances during the fatigue test, so a replacement specimen was tested. This replacement Pathfinder II passed all the tests, so the previous foot was excluded from any subsequent analysis.

Table 4.1: Characteristics of prosthetic feet tested

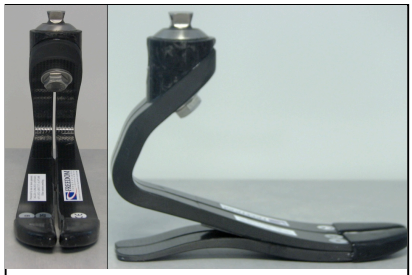

Figure 4.1: Freedom Sierra FS1

Figure 4.2: Ossur VSP

Figure 4.3: Ohio Willow Wood Pathfinder II

Manufacturer	Model	Activity level	size	Material	category	Weight limit
Freedom	Sierra FS1	High	26 cm	Carbon fiber	9	365lbs
Ohio Willow Wood	Pathfinder II	High	26 cm	Carbon fiber& pneumatic heel spring	9	350 lb
Ossur	Re-flex VSP	High	26 cm	Carbon fiber &compression spring	9	365lbs

High activity level include rigorous activity, competitive sports, running, power lifting, and snowboarding.

Table 4.2: Test Results

Prosthetic Foot	Proof Test	Ultimate Test	Fatigue Test	Post-Fatigue Proof Test
Freedom Sierra 1	Pass	Pass	Pass	Pass
Freedom Sierra 2	Pass	Pass	Pass	Pass
Freedom Sierra 3	Pass	Pass	Pass	Pass
Ossur VSP 1	Pass	Pass	Pass	Pass
Ossur VSP 2	Pass	Pass	Pass	Pass
Ossur VSP 3	Pass	Pass	Pass	Pass
OWW Pathfinder II 1	Pass	Pass	Pass	Pass

OWW Pathfinder II 2	Pass	Pass	Pass	Pass
OWW Pathfinder II 3	Pass	Pass	Pass	Pass

Stiffness and creep at the heel and forefoot was calculated for each specimen during the pre- and post-fatigue proof tests. Stiffness was calculated by taking the slope of the loading portion of the force-displacement curves. Creep was determined by taking the difference in displacements between the beginning and end of the proof tests. The results of which can be seen in the figures below:

Figure 4.4: Forefoot Stiffness Results

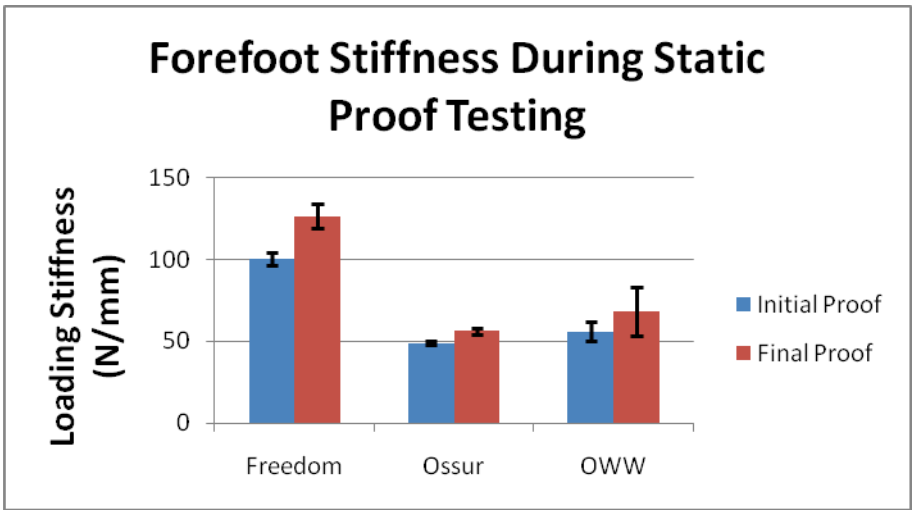

Figure 4.5: Heel Stiffness Results

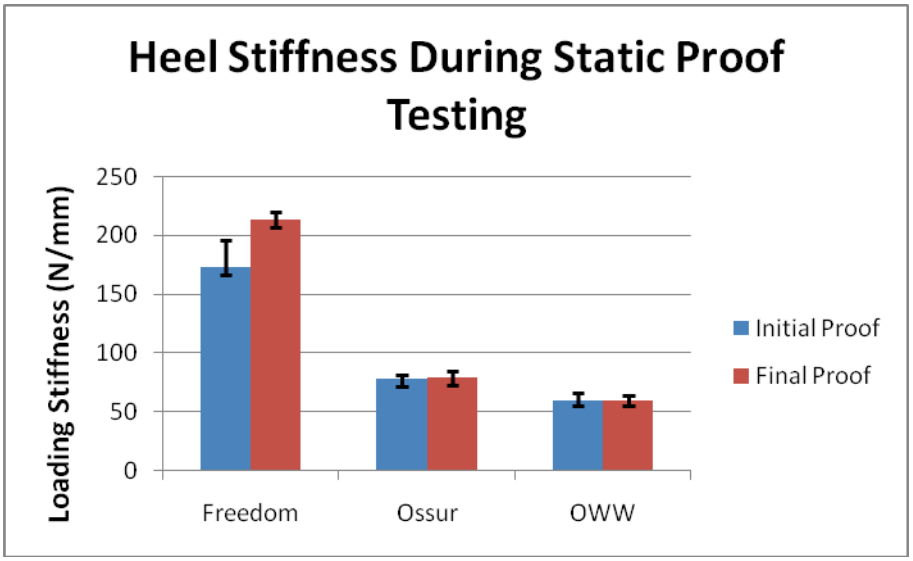

Figure 4.6: Forefoot Creep Results

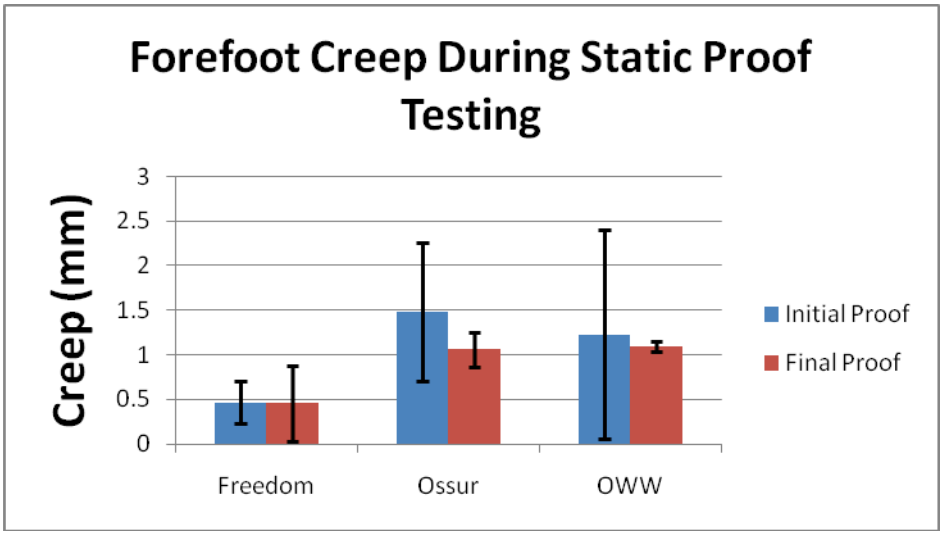

Figure 4.7: Heel Creep Results

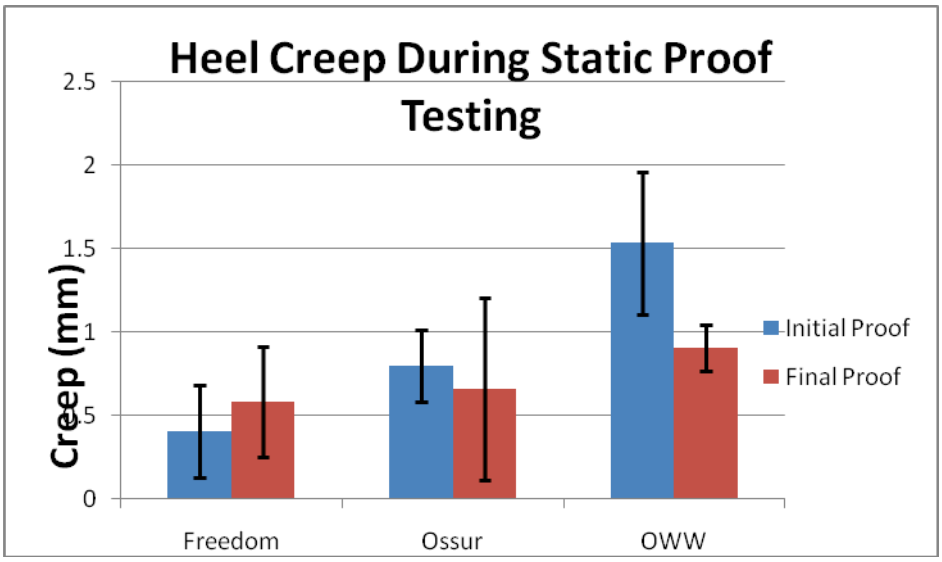

To investigate whether or not a given model foot suffered internal or non-visible damage during the cyclic test, a two repeated measures ANOVA with a Tukey post-hoc test were used to determine any differences in both stiffness and creep between the initial static proof test and the final static proof test. A non-parametric Kruskal-Wallis test was used to determine if the models of prosthetic feet were affected differently by the cyclic portion of the standard by comparing stiffness and creep experienced during the final static proof test. All statistical analyses were done with a significance level of 0.05.

While the Kruskal-Wallis test, which compared post-fatigue stiffness and creep between models of feet, showed no significant results, The repeated measures ANOVA revealed several significant differences in creep or stiffness between pre- and post-fatigue testing for a given model of foot.

Table 4.3: Results of the Repeated Measures ANOVA

Prosthesis	Section	Parameter	P value	Post-hoc Test Result
Sierra	**Forefoot**	**Stiffness**	0.001	Initial < Final
		Creep	0.292	NA
	Heel	**Stiffness**	0.002	Initial < Final
		Creep	0.301	NA
Re-flex VSP	**Forefoot**	**Stiffness**	0.001	Initial < Final
		Creep	0.042	Initial > Final
	Heel	**Stiffness**	0.801	NA
		Creep	0.043	Initial > Final
Pathfinder II	**Forefoot**	**Stiffness**	0.017	Initial < Final
		Creep	0.571	NA
	Heel	**Stiffness**	0.795	NA
		Creep	0.143	NA

While some of the results of this statistical analysis are not what was expected, such as post-fatigue stiffness being greater than pre-fatigue, these results could have been affected by the low sample size and the differences in design and materials used in the different models of feet.

Plans:

Testing of all nine prosthetic feet is complete and the data has been analyzed, the results of which were submitted and published in the scientific journal Prosthetics and Orthotics International. Since no failures occurred during the ISO testing of the feet and the results of the statistical analysis were inconclusive, more rigorous tests will be developed in order to simulate the failures that clinicians and prosthetic users experience in the field. This will include developing tests that investigate the behavior of the feet under torsional loads and abnormal environmental conditions, such as excessive heat and cold. Currently, the testing apparatus and protocol is being redesigned to accommodate a combination of axial and torsional loads while more prosthetic feet have been purchased to obtain fresh samples to carry out this combination of loading. The torsion testing portion of the study will be based on testing recommendations published by the American Orthotic and Prosthetic Association (AOPA), since the ISO does not include torsion test guidelines for prosthetic foot units in ISO:10328. Four new prosthetic feet have been obtained to pilot this axial-torsional testing, which, in addition to the three models used previously, includes the LP Vari-flex from Ossur. This foot is being added to the study based on input from clinicians that indicate this foot is often prescribed to individuals who perform activities involving twisting at the ankle, such as golf, more frequently than normal prosthesis users.

Project 4. Prosthetic hardware testing

Milestones	**Progress**
Design and assemble system for prosthetic life-cycle testing.	• Complete
Develop data acquisition system and complete pilot testing	• Complete
Acquire prosthetic feet and develop fixturing for life-cycle testing	• Complete
Complete testing of prosthetic feet.	• Complete
Data analysis and preparation of journal paper submission	• Complete. Journal paper published in Prosthetics and Orthotics International
Upgrade testing system to accommodate torsion testing	• Complete
Acquire prosthetic feet to pilot torsion testing	• Complete: Ohio Willow Wood Pathfinder II, Freedom Sierra, Ossur Re-Flex VSP, and Ossur LP Vari-Flex
Development of fixture to allow for torsional testing of prosthetic feet	• Ongoing
Development of testing protocol that combines axial and torsional loading	• Ongoing
Carry out pilot testing combining previous ISO standard tests with torsion tests detailed by AOPA	• Ongoing

Personnel Supported by this Contract

Program Director
Douglas Weber, PhD.

Investigators
Michael Boninger, Ph.D.
Jennifer Collinger, Ph.D.
Rory Cooper, Ph.D.
Tracy Cui, Ph.D.
Carl Lagenaur, Ph.D.
Jon Pearlman, Ph.D.
Wei Wang, Ph.D.
Ross Zafonte, D.O.

Postdoctoral Associates and Scholars
Robert Gaunt, Ph.D.
Christi Kolarcik, Ph.D.
Ramana Vinjamuri, Ph.D.
Sergiy Yakovanko, PhD
Ling Zhang, Ph.D.

Research Staff

Ingrid Albrecht	Lab Manager & Technician
Robin Ashmore	Software Engineer
Elizabeth Harchick	Research Coordinator
Zachery Mason	Bioengineer
Christian Niyonkuru	Biostatistician
Hetul Patel	Systems Programmer
Jeremy Puhlman	Bioengineer
Erika Rost	Research Technician
Tyler Simpson	Research Engineer

Graduate Student Researchers
Nicolas Albas
Chris Ayers
Dennis Bourbeau
Alan Degenhart
Giovanna DiStefano
Amit Kumar
Zach Merrill
Gustavo Sudre
Chung-Ying Tsai

Undergraduate Student Aides
Sean Brice
Emily Foley
Brianne Miller
Danielle Rager
Robert Schwartz
Rishi Sethi